Identifying maize architectural ideotypes through 3D structural model validated in the field: Assessing the impact of plant architecture and sowing pattern to improve canopy light regime

Mario Serouart, Raúl López-Lozano, Brigitte Escale, Maëva Baumont, Jean-Charles Deswarte, Lucas Samatan Bernigaud, Marie Weiss, Benoit de Solan

Computers and Electronics in Agriculture 229 (2025) 109694

Contents lists available at ScienceDirect

Computers and Electronics in Agriculture

journal homepage: www.elsevier.com/locate/compag

Original papers

Identifying maize architectural ideotypes through 3D structural model validated in the field: Assessing the impact of plant architecture and sowing pattern to improve canopy light regime

Mario Serouart [a,b,*], Raúl López-Lozano [a], Brigitte Escale [c], Maëva Baumont [c], Jean-Charles Deswarte [d], Lucas Samatan Bernigaud [b], Marie Weiss [a], Benoit de Solan [b]

[a] INRAE, UMR EMMAH, UMT CAPTE, 228 route de l'aérodrome, 84914 Avignon, France
[b] Arvalis, UMT CAPTE, 228 route de l'aérodrome, 84914 Avignon, France
[c] Arvalis, Ecophysiology, 21 Chemin de Pau, 64121 Montardon, France
[d] Arvalis, Station Expérimentale, 91720 Boigneville, France

ARTICLE INFO

Dataset link: https://github.com/mserouar/CORNIBU

Keywords:
Light
Maize
Modeling
Phenotyping
Plant architecture
Plasticity
Sensivity analysis

ABSTRACT

This study explores the influence of in-field maize plant architectural parameters (leaf inclination, curvature, orientation) and sowing patterns (plant density from 6 to 12 plts m^{-2}, row spacing from 0.4 to 0.8 m) on canopy light conditions. A new three-dimensional (3D) maize architectural model -CORNIBU, integrated with a canopy light regime computation model- was able to describe phenotypic space with a relatively low number of input parameters. The reliability of CORNIBU to describe the actual variability of daily $fIPAR$ (fraction of Intercepted PAR) depending on the sowing pattern and plant architecture was evaluated by generating digital canopies of five actual maize hybrids from a field experiment. The predicted daily $fIPAR$ from CORNIBU digital canopies and the field-measured $fIPAR$ from hemispherical photographs on actual maize canopies exhibited a significant and positive correlation ($R^2 \sim 0.6$), when calibrating the leaf phyllotaxy parameter from nadir gap fraction. Then, an *in silico* experiment conducted with CORNIBU permitted to identify the architectural ideotypes maximizing canopy light interception ($fIPAR$) and canopy light distribution ($fILA$, the fraction of Illuminated Leaf Area). This analysis highlighted a trade-off between $fIPAR$ and $fILA$, therefore any architectural ideotype cannot maximize both variables. Deeper light distribution would be achieved with more erectophile leaves and leaves orientation following an almost distichous phyllotaxy, whereas greater light interception would be achieved with more pronounced planophile leaves and random leaf orientation. The incorporation of photosynthetic light-responsive curves to estimate canopy daily photosynthesis provided additional insights to understand the trade-off between $fIPAR$ and $fILA$. Our findings indicate that the form of the hyperbolic function, i.e of the light-response curve, determines the optimal balance between $fIPAR$, $fILA$ and the resulting architectural ideotypes. Plant architectures with a higher light interception -planophile leaves- maximize daily canopy photosynthesis when the light-response function is more linear, whereas a more asymptotic curve determines that ideotypes where incident light is more uniformly distributed through the foliage depth -erectophile leaves- are those that optimize daily canopy photonsynthesis. Finally, our analysis highlights that squared sowing patterns (plant spacing within rows is close to row distance) benefit canopy-level photosynthesis by decreasing mutual shading between plants within the same row, as compared to traditional rectangular patterns where row distance is 4 to 8 times higher than plant spacing.

1. Introduction

Maize (*Zea mays L.*) is the most important cereal grown globally, with a production of 1.2 billion tons of grain per year (FAO, 2023). Since the 1960s, maize yields at the global level have followed a positive trend resulting from improvements in cultural practices and incorporation of high-yielding varieties (Eliazer Nelson et al., 2019). Tolerance of maize to high plant density is one of the factors that has favored such yield increase (Berzsenyi and Tokatlidis, 2012).

* Corresponding author at: INRAE, UMR EMMAH, UMT CAPTE, 228 route de l'aérodrome, 84914 Avignon, France.
E-mail address: mario.serouart@inrae.fr (M. Serouart).

https://doi.org/10.1016/j.compag.2024.109694
Received 12 March 2024; Received in revised form 23 October 2024; Accepted 20 November 2024
Available online 30 December 2024

Tolerance depends on the ability of the plants to optimize the access to resources when increasing intra-specific competition (Sangoi, 2001). In non-limited water and nitrogen growing conditions, incoming light may limit individual plant growth and yield due to mutual shading as plant density increases (Maddonni et al., 2001b; Timlin et al., 2014). The trade-off between plant density, individual plant growth and yield depends on both plant architecture and spatial arrangement -the arrangement of plants within the canopy- and must be carefully considered when evaluating the impact of plant density in intra-specific competition for light in maize crops. Indeed, under the same plant density, row spacing plays a significant role in determining light interception and penetration within the canopy (López-Lozano et al., 2007; Maddonni et al., 2001a). Standardized practices in maize -0.7, 0.75 m row distances- that are still used nowadays, were partly due to the use of animal-drawn farm equipment facilitating inter-row tillage (Sharratt and McWilliams, 2005) and may not be optimal nowadays from the perspective of maximizing light interception and growth at higher plant densities.

Actually, the possible benefit of narrow spacing (<0.7 m) in enhancing maize light interception has already been evaluated in several studies (Testa et al., 2016; Gao et al., 2021; Li et al., 2021), but there is no consensus about its impact on final yield. The effect of plant density and row spacing on yield also depends on the phenotypic plasticity of maize to cope with intra-specific competition for light. Plasticity is triggered by resource limitation and environmentally induced stress factors. It includes, for example, changes in leaf dimension, stem diameter, height and leaves inclination/orientation, with substantial differences among cultivars (Maddonni et al., 2002; Serouart et al., 2023). Indeed, most of the mentioned studies about the contribution of canopy structure to improve maize yields are focused on understanding the impact of architectural variables in total light interception (i.e. in the fraction of intercepted photosynthetically active radiation, or $fIPAR$). Nevertheless, the recent study of Perez et al. (2019) highlighted the key role played by plant architectural traits that modify light distribution within the canopy -not simply light interception- in the breeding process towards recent maize cultivars that are tolerant to high plant density. In field trials, measuring realistically the incident light distribution through the canopy is very challenging.

Plant three-dimensional (3D) models were conceived to overcome this limit and realistically simulate crop architecture by studying in detail light-plant interactions. Such models have an enormous potential to describe the role played by both plant morphological traits and stand structure in architecture-driven processes such as light interception, light absorption and canopy-level photosynthesis. The advantages of including 3D plant models in prospective studies to disentangle the role of plant stand architecture in canopy light regime studies rely on, essentially, three points. First, they can model with realism the 3D plant and canopy architecture through a number of structural input variables that can be measured in the field. Second, they permit simulating a large phenotypic variability, combined with different stand parameters (e.g. plant density and row spacing), difficult to achieve only by means of traditional field experiments. Third, when coupled with physically-based algorithms to model realistically light-plant interactions, plant 3D models enable the computation of essential indicators that cannot be easily measured *in situ* to understand light distribution within the canopy and canopy-level photosynthesis (Fournier et al., 2016).

The main goal of this study is assessing the influence of maize plant architecture and the sowing pattern on light interception, distribution and photosynthesis at the canopy-level by using a new 3D maize model coupled with a radiative transfer model. More specifically, this study tries to identify the maize architectural ideotypes and the sowing patterns that optimize canopy light regime through different light indicators. To achieve that goal, the study addresses three specific objectives. The first objective is developing and validating a new maize 3D model -named CORNIBU- that permits to explore easily the phenotypic space of maize architectural traits -mainly leaf dimensions, inclination, curvature and orientation- with a limited number of parameters, that all can be measured in the field. The validation is achieved by comparing *in situ* -in a field trial- $fIPAR$ measurements for different maize cultivars and sowing patterns, with $fIPAR$ predicted from CORNIBU, in same experimental conditions. The second objective is quantifying the relative contribution of the different plant architectural traits and the sowing pattern through an *in silico* experiment in determining light interception ($fIPAR$) and light distribution ($fILA$, i.e. the fraction of the illuminated leaf area). Finally, the third objective is characterizing the link between light interception and light distribution to determine canopy-level photosynthesis under different maize plant and stand architectures. Special attention is paid to understand how the possible different shapes of the photosynthetic light-response curves at the leaf level (e.g. Farquhar et al., 1980; Song et al., 2023; Wang et al., 2012) determine the optimal plant architecture (ideotype) and the sowing pattern that maximize photosynthesis at the canopy scale.

This paper is structured as follows. Section 2 presents the CORNIBU maize model, the field experiments necessary to validate the model, and the *in silico* experiment conducted to understand the role of plant and stand architectural parameters in light interception, distribution and canopy photosynthesis. In Section 3, we first present the accuracy of the CORNIBU fitting to simulate actual maize architectural parameters (e.g. individual leaves length, leaves inclination and curvature, leaves orientation) and the daily $fIPAR$ using data from the field experiments. Then, we detail the results of the *in silico* analysis about the role of the plant architectural parameters and the sowing pattern (plant density and row spacing) in determining light interception, distribution, and canopy photosynthesis. The discussion in Section 4 elaborates on three main issues: (i) the reliability of CORNIBU to model realistically light interception of actual maize canopies; (ii) the observed trade-off between light interception and light distribution resulting from plant architectural parameters and their role in canopy photosynthesis; and (iii) the contribution, according to the *in silico* experiment, of adapting row distances to enhance canopy-level photosynthesis. The paper finishes with some concluding remarks in Section 5.

2. Materials and methods

2.1. Experimental set-up

A field experiment was conducted in 2022 at the Montardon station of the Arvalis Institut (located at 43° 22′ N, 0° 20′ W) (Fig. 1, left). A panel of five commercial maize hybrids belonging to the same precocity group were grown. To prevent any possible conflicts with trademarks or proprietary information, the name of five maize hybrids are replaced by ficticious ones: DANTES, IGNATIUS, MONTAG, ESMERALDA, and WINSTON. Maize was sown on 1st June 2022 and was grown under non-limited water and nitrogen conditions. Among the five hybrids, some *a priori* differences exist regarding plant architecture (according to breeders), particularly canopy height and leaf inclination.

The five hybrids were sown in four different sowing patterns, by varying both, the plant density (6 and 12 plants m^{-2}) and the row spacing (0.4 and 0.8 m). These four patterns resulted in a gradient of Rectangularity from 1 to 8, explicitly displayed in Fig. 1, right. To characterize these sowing patterns, we computed the Rectangularity (R), defined as the ratio between row spacing and plant spacing within the same row (Willey and Heath, 1969; Maddonni et al., 2001b).

The combination of the five maize hybrids (G) and the four sowing patterns (R) resulted in 20 GxR combinations replicated in a 3-block experimental design, thus resulting in a total of 60 microplots. To facilitate sowing operations each R treatment was located in a single trial column, with hybrids distributed randomly within each block. Microplots were 6 m long by 4 m wide, corresponding to 4 rows and 8 rows, respectively for row spacing of 0.8 and 0.4 m. Rows were oriented, approximately in the NE-SW direction (row azimuth was 48.37°). Additional buffer plots were sown at each side of the experiment to prevent possible border effects.

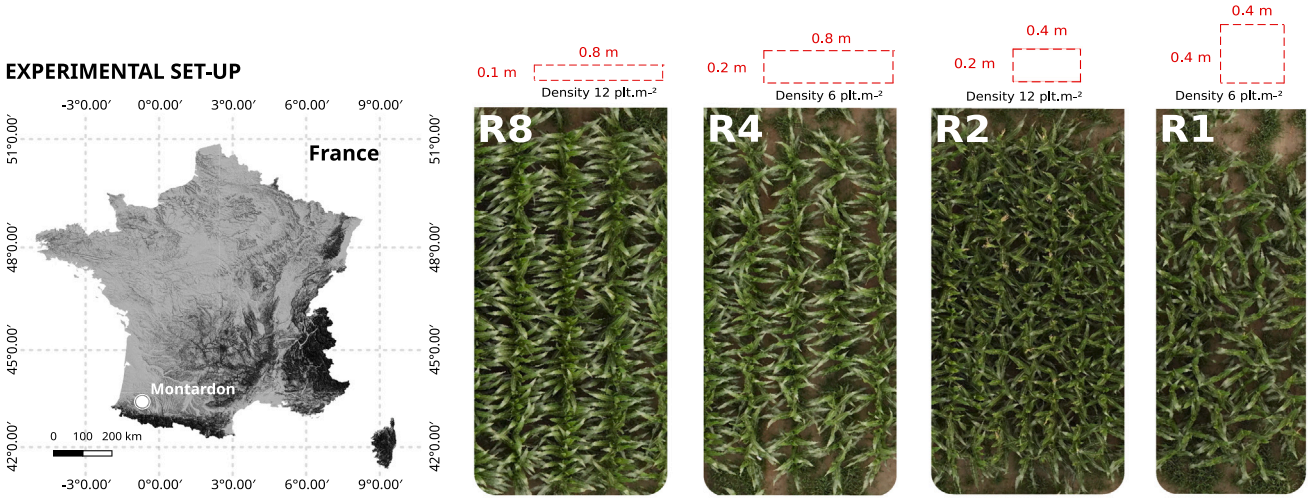

Fig. 1. Left - Experimental site of Montardon location and Right - Unmanned Aerial Vehicle illustration of the four rectangularity levels investigated.

Table 1
List of architectural traits measured in the Montardon experiment.

Trait	Type of measurement	Way of acquiring	Phenological stage
Leaf dimensions	In situ, manual	–	R1-R2
Leaves insertion height	In situ, manual	–	R1-R2
Leaves orientation	Non-destructive, automatic from RGB Images	ALAEM algorithm (Serouart et al. 2023)	V12-14
Leaf phyllotaxy	Destructive, manual	–	R1-R2
Leaf inclination and curvature	Destructive, manual from RGB Images	PoPCorn algorithm	R1-R2
Canopy gap fraction	Digital hemispherical photographs	POVRay | FishEye	R1-R2

2.2. Measurement of architectural variables from actual maize hybrids in the field

A summary of the architectural variables measured in the Montardon experiment is given Table 1.

2.2.1. Distribution of leaves orientation

The distribution of leaves orientation was measured from vertical RGB images using the ALAEM algorithm (Serouart et al., 2023). Six vertical images were acquired on the central rows of each of the 60 microplots, with a portable handheld phenotyping device called LITERAL (developed by the Arvalis Institut, and funded by the French CASDAR program). The LITERAL device consists of a pole equipped with two RGB cameras (SONY RX0 II) viewing at nadir. A digital inclinometer enables verifying the camera inclination in real-time during data acquisition. The acquisition of vertical images took place on 11th July 2022 (650 °Cd), when maize was at the phenological stage V12-V14 (twelve to fourteen ligulated leaves, Ritchie and Hanway (1982)).

The ALAEM algorithm computes individual leaves azimuth by detecting automatically the leaves midribs in RGB images of the canopy. The output of ALAEM for the six images per microplot provided a distribution of leaves orientation of the top layer of the canopy. The observed leaves orientation distributions provided by the ALAEM algorithm are shown in Figure S1 (Supplementary Materials).

2.2.2. Leaves inclination and curvature

Leaves inclination trajectories were measured manually on individual plants. At the R1-R2 stage (4th August 2022), 6 plants per microplot were cut at the base of their stem and progressively transported to the laboratory. Once there, each plant was placed vertically with the assistance of a metal support. Each plant was then photographed in front of a vertical checker board background with a Sony Alpha RGB camera oriented horizontally. To prevent from leaf rolling, which could alter leaves inclination (Baret et al., 2018), the photographs were captured within a maximum of 20 min following the cutting of the plants in field. Then, the PoPCorn software, developed by the CAPTE team (available at https://www.paca.inrae.fr/emmah/Production-Documentation/Outils-et-modeles/PoP-Corn) was used to digitize the stem and leaves trajectories manually from the photographs. Thanks to the checkered board, used as background, the photographs could be converted into an orthonormal image, which permitted to compute the actual inclination and curvature of every single leaf in the plant.

2.2.3. Leaf dimensions and insertion height

On the same date as leaves inclination measurements (stage R1-R2), the length and width of every alternate leaf (from the top leaf) were measured on a sample of 12 plants per microplot, distributed in two groups of 6 consecutive plants in the central rows of the microplot. The manual measurements were non-destructive, conducted with a flexible measuring ruler. Similarly, the height from the ground of leaves insertion were also measured. The leaf dimensions of not measured alternate leaves were computed by extrapolating the values of those measured using a linear function. This extrapolation was used to calibrate our model on what regards Leaf Area Index (LAI) and compare the virtual canopy faced to the real one, i.e. not being dependant of the alternate manual leaf measurement strategy.

2.2.4. Canopy gap fraction

Canopy gap fraction was measured *in situ*, using Hemispherical photographs. On every plot, 40 images were acquired using an Alpha 5000 RGB (Sony Inc, Japan) with a fish-eye lens (Lensbaby, US). The images were taken placing the camera at ground level and looking upwards. The set of 40 images per microplot were divided into five transects of 8 pictures taken with the aid of a wooden ruler to sample regularly the space between rows. The optical system camera and fish-eye lens were calibrated in laboratory following the methodology described in the CAN-EYE software (https://www6.paca.inrae.fr/can-eye/Documentation/Documentation), to retrieve the coordinates in image units of the optical center and the 2nd degree polynomial function

Table 2
List of input architectural variables for the 3D maize model proposed and proposed intervals.

	Symbol	Name	Units	Intervals
Plant dimensions/leaf area	H_{max}	Maximum plant height	m	[2.5–4]
	N_{max}	Maximum number of leaves	–	[14–18]
	S_{max}	Maximum leaf area (one-sided) per plant	m^2	[0.5–0.7]
Stand	D	Plant density	plants m^{-2}	[6–12]
	dr	Row spacing	m	[0.2–1.0]
Leaves orientation	ϕ_p	Mean plant azimuth relative to rows direction	°	[0–90]
	$\sigma_{\phi,p}$	Standard deviation of mean plant azimuth	°	[0–90]
	$\sigma_{\phi,l}$	Standard deviation of individual leaves orientation against mean plant azimuth	°	[0–90]
Leaves inclination and curvature	$\theta_{i,top}$	Inclination angle at insertion of the top leaf	°	[0–90]
	$\theta_{i,base}$	Inclination angle at insertion of the base leaf	°	[0–90]
	$\Delta\theta_{base}$	Difference in inclination between the insertion point and the tip of the base leaf	°	[0–240]
	$L_{\Delta\theta}$	Relative leaf length at which inflection point in inclination occurs	–	[0–1]

that permits to associate a viewing direction (zenith angle θ_v, azimuth angle ϕ_v) to every pixel in the image. Images were taken, as much as possible, during the morning and evening to avoid lens flare due to the sun shining directly above the canopy.

The Hemispherical images were cropped to constraint the field of view between 0–60° θ_v to avoid problems of bias in the gap fraction due to the degradation of resolution in the hemispherical photographs at large viewing angles. The images were then classified into 'vegetation' and 'sky' using the SegVeg algorithm (Madec et al., 2023; Serouart et al., 2022). The images were divided into sectors of 2.5° (azimuth ϕ_v) × 5° (zenith θ_v) to calculate the gap fraction (P_0) of every sector as the proportion of pixels classified as 'sky'. The resulting gap fraction values per image were averaged per GxR treatment (120 images, 40 per plot × 3 replicates) to retrieve the mean canopy gap fraction. An example of the resulting canopy gap fraction is given in Figure S2.

2.3. Modeling light interception in maize canopies: the CORNIBU model

The present study relies on a newly developed maize architectural model coupled with the Caribu algorithm (Chelle and Andrieu, 1998), the latter including ray-tracing and nested radiosity methods to simulate light regime over 3D scenes. The architectural model, detailed along this section, coupled with the Caribu algorithm is called CORNIBU, and is publicly accessible via Github (https://github.com/mserouar/CORNIBU).

2.3.1. Description of the 3D architectural maize model

The maize 3D architecture model used in this study simulates different structural characteristics of maize plants: leaves shape and dimensions, leaves inclination and curvature, insertion height and plant/leaves orientation. Compared to previous models (Fournier and Andrieu, 1998; España et al., 1998; López-Lozano et al., 2007), this new one presents a good compromise between details in describing architectural characteristics (like leaves orientation, not sufficiently considered in previous models) while keeping a reduced number of input variables accessible from field measurements. The list of architectural variables is given in Table 2, and a graphic description of such variables is given in Fig. 2. For the sake of readability, this section describes the main principles of the CORNIBU model parameterization. The full set of model formulae is given in the Supplemental Materials ST1 Table.

The plant dimensions and leaf area are controlled by the maximum plant height (H_{max}), maximum leaf area per plant (S_{max}) and the maximum number of leaves (N_{max}). The insertion height of each individual leaf is determined by an allometric function depending on H_{max}, S_{max} and N_{max}, reported by España et al. (1998). According to their work, a power function provides a good approximation between leaf order and leaf height, with h_1 -the first leaf near the ground- is fixed at 0.015 m. See Supplementary Table 1 -ST1- Eq. h_i.

To derive individual leaf size, i.e. width (w_i), length (l_i) and consequently area (S_i), several similar allometric relationships were explored. The maximum leaf width was described by a polynomial function between the leaf order and leaf width where, again, the first order w_1 was fixed at 0.015 m (see ST1 Eq. w_i). Leaf length on its side was approximated by a linear function up to the first seven leaves. For the remaining leaves, according to N_{max}, a parabolic function between leaf order and length is assumed (see ST1 Eq. l_i). Again, the first leaf length l_1 was averaged at 0.04 m.

The methodology employed to depict organ geometry, especially leaf lamina shape and its alterations within plant topology, relied on leaflet shape of oil palm trees (Perez et al., 2016, ST1 Eq. Leaf lamina shape width ratio). In essence, it employs a mathematical model to portray the radial structure of a leaf lamina, enabling a thorough characterization of leaf morphology. Briefly, the leaf lamina is spread out onto a flat plane surface, the central rib being the symmetry axis. Thus, we only consider half the leaf lamina in our model, that can be represented as a parabolic function where we considered the relationship between the width of the leaf on y-axis at a given length point on x-axis. To preserve the previously calculated individual surface areas of leaves -depending of leaf length, width and S_{max}-, a computational process was implemented to ensure that the computed leaf lamina shape agrees with the targeted leaf area. This was done thanks to *trapz* function of the NumPy python package that uses numerical integration (through area under the curve) to adjust the shape parameters, so that the computed leaf area matches the given value.

Each plant in the stand has an individual orientation relative to the row direction, which is drawn from a normal distribution at the stand scale determined by the variables ϕ_p and $\sigma_{\phi,p}$, which are, respectively, the mean and standard deviation of plant azimuth. These two variables permit to describe, at the stand level, a possible preferential orientation of plants exhibited by some maize hybrids in high rectangularity patterns (Serouart et al., 2023). Furthermore, at the plant level this time, the variable $\sigma_{\phi,l}$ controls leaves phyllotaxy by determining the standard deviation of individual leaves from the plant azimuth (Fig. 2). A perfect distichous phyllotaxy (i.e. with a difference of 180° between the azimuth of two consecutive leaves) corresponds to $\sigma_{\phi,l} = 0$. For more details, please refer to ST1 Eq. Leaf orientation.

To model leaves trajectories -inclination and curvature-, the variables $\theta_{i,base}$ and $\theta_{i,top}$ are used to determine the inclination of the bottom and top leaves, respectively, at their insertion points (the angle at which the leaf is attached to the stem). A linear interpolation between $\theta_{i,base}$ and $\theta_{i,top}$ is assumed to adjust the inclination for every leaf order, according to the difference between $\theta_{i,base}$ and $\theta_{i,top}$. The leaf curvature, in turn, is calculated starting with the first base leaf and then extrapolated to other leaf ranks. This latter is determined and initialized by the input variable $\Delta\theta_{base}$, which corresponds to the angular difference -in degrees- between the inclination at the insertion point and the leaf tip. Additionally, the curvature is also influenced by $L_{\Delta\theta}$, which refers to the relative midrib length where the inflection point occurs.

Thus, for a given rank, the $leaf_{tip}$ angle -which influences the final leaf curvature angle- is set with a log-sigmoid function based on $\Delta\theta_{base}$, as recommended by Perez et al. (2016) and Boudon et al. (2020) in ST1 Eq. $leaf_{tip}$ angle. Then, based on given coefficients and previously computed $leaf_{tip}$ angle, the curvature of the leaf can be provided

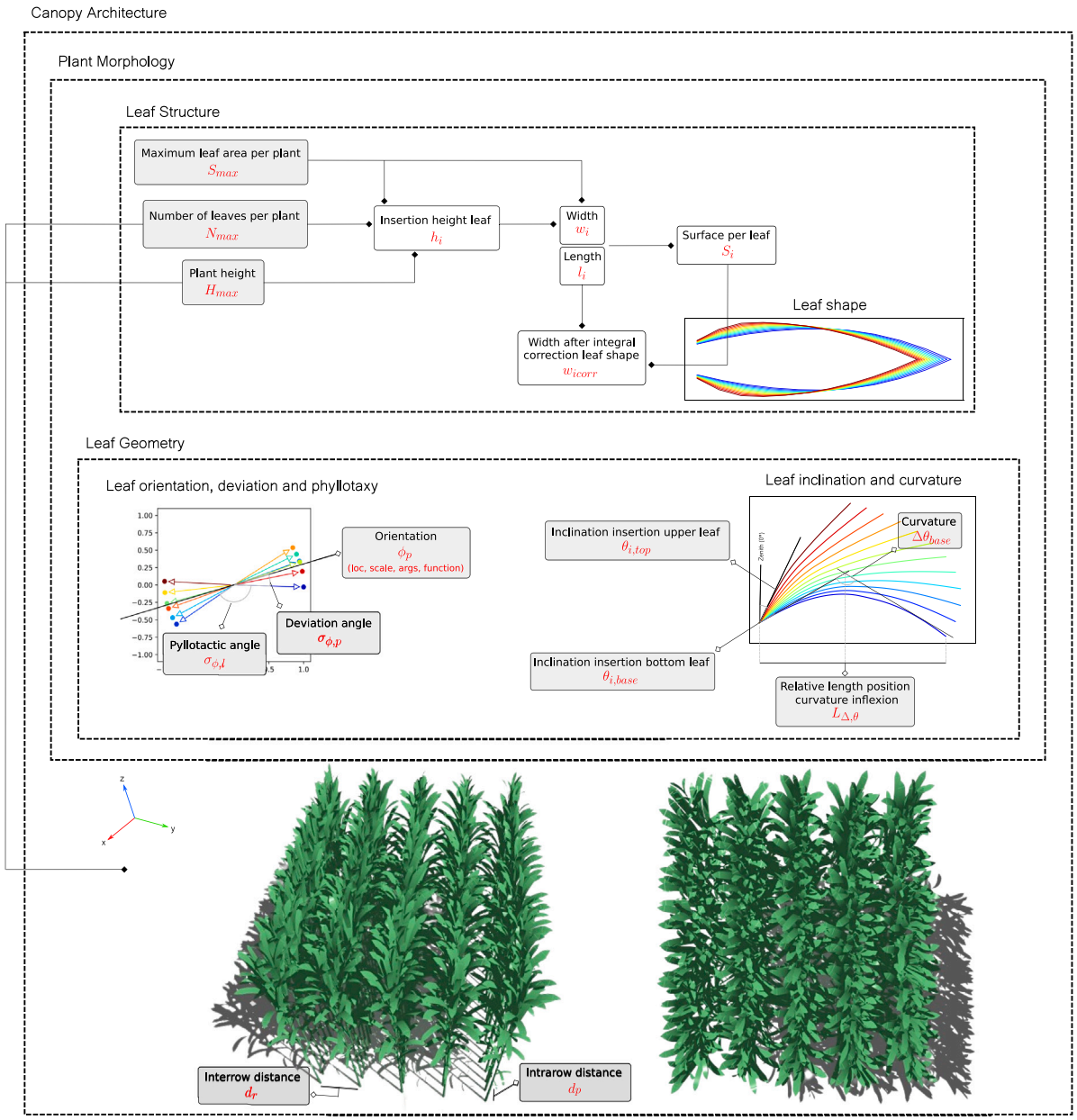

Fig. 2. Overview of inputs, related parameters and final canopy example of CORNIBU model.

(through several segments along the leaf length, $curvature_{portion_1}$ and $curvature_{portion_2}$ in ST1). Finally, these segments are adjusted using the coefficient $L_{\Delta\theta}$ related to the inflection point. This parameter is assumed to be constant for all leaves. The x- and y- coordinates along the leaf's edge are obtained by combining segment lengths and angles. All these considerations ensure a gradual and realistic change in the leaf bending angle, resulting in a well-scaled and realistic representation of the plant profile from base to top.

Even if $L_{\Delta\theta}$ parameter is fixed, because of the varying nature of $leaf_{tip}$ which is only initialized by $\Delta\theta_{base}$, it is still possible -for example- to model a greater curvature at the bottom of the stratum compared to the top.

2.3.2. Modeling light regime on 3D scenes

The Caribu model (Chelle and Andrieu, 1998) was used to compute different indicators of light regime in the canopy. The Caribu model is accessible in the Git repository hyperlink : https://github.com/openalea-incubator/caribu/.

The fraction of intercepted photosynthetically active radiation ($fIPAR$) is calculated by using a projective method (the Z-buffer method, Khan et al. (2013)). In such method the set of triangles in the 3D scene is projected onto a regular grid in a plane perpendicular to the incident light direction. An object -and its corresponding pixel within final image- is displayed only if its depth is less than those already present in the buffer memory. This principle ensures that only the visible surfaces contribute to the final image, handling occlusions. The $fIPAR$ is the ratio between the number of grid points above the ground distance and the total number of grid points.

The Caribu module computes, as well, the intensity (E_i) of the incident light on every triangle facet i, based on the phase angle between the facet and the incoming light direction (normalized between 0 and 1). Then, the fraction of illuminated leaves ($fILA$) is computed as:

$$fILA = \frac{\sum_i^n \forall i S_i E_i > 0}{S_c} \quad (1)$$

where S_i is the area of illuminated facets ($E_i > 0$) and S_c is the total leaf area.

To avoid border effects, in the computation of $fIPAR$ and $fILA$, the 3D scene was replicated indefinitely. Both, $fIPAR$ and $fILA$ were computed for direct (black sky) and diffuse light (white sky). For the computation of diffuse light, Caribu simulates a set of light sources from a sky vault discretized in 46 solid angle sectors, including five zenith angles known as turtle computation (Dulk, 1989). The contribution of each sky sector to the incoming diffuse light is then weighted according to the standard overcast sky radiation distribution.

The two indicators, $fIPAR$ and $fILA$, are complementary to understand light regime in the canopy as they describe, respectively, the total light interception and how that intercepted light is distributed inside the canopy foliage. Indeed, the distribution of incident light is an important factor to characterize the use of light at the canopy scale, as the light response of photosynthesis is non-linear (Farquhar et al., 1980; Yin and Struik, 2009). It then *a priori* may favor those canopies where incoming light is more evenly distributed over the foliage. To understand the possible effect of architectural parameters in photosynthesis, canopy-level photosynthesis was computed from Caribu outputs:

$$A_c = \frac{\sum_i^n A_i * S_i}{S_c} \tag{2}$$

where A_c is instantaneous canopy-level photosynthesis and A_i is the instantaneous photosynthesis on facet i, which is computed using the nonrectangular hyperbola shape:

$$A_i = \frac{\alpha I_i + A_{max} - \sqrt{(\alpha I_i A_{max})^2 - 4\kappa\alpha I_i A_{max}}}{2\kappa} - Rd \tag{3}$$

In such model, A_{max}, α, κ and Rd are, respectively, the maximum photosynthetic rate [in µmol (CO_2) m^{-2} s^{-1}], the apparent quantum yield [µmol (CO_2) m^{-2} s^{-1}], the convexity parameter (unitless), and the dark respiration [in µmol (CO_2) m^{-2} s^{-1}], all of them parameters that can be fitted from *in vivo* measurements of leaf photosynthesis. The variable I is the absorbed photosynthetic photon flux density ($PPFD$) in facet i, which is computed as:

$$I_i = Q_{PAR} \cdot \left[f_d \cdot E_{i,d} + (1 - f_d) \cdot E_{i,s}\right] \cdot a \tag{4}$$

where Q_{PAR} is the total incoming PAR $PPDF$, f_d is the diffuse fraction of incoming light, $E_{i,d}$ and $E_{i,s}$ are the relative incident light intensity of diffuse (d) and direct (s) radiation, computed from Caribu, and a is leaf absorbance in the PAR region (0.85). For the simulation of daily-integrated canopy photosynthesis A_d (in the *in silico* experiment with the maize canopy) the instantaneous A_c is integrated over the day, every hour.

The curvature of photosynthetic light-response curves is determined by environmental conditions such as temperature, water stress or leaf age. To investigate the impact of the curvature of the light-response curve in the optimal architecture that maximizes canopy photosynthesis, we considered two different scenarios, based on published work (Fig. 3). The first curve -referred as 'non-saturated light response'- is taken from the work of Wang et al. (2012), and describes an almost linear relationship between $PPDF$ and A_c until a saturation plateau at 1500 µmol m^{-2} s^{-1}. The originally calibrated parameters are 0.035, 40.2, 1.87 and 0.90 for α, A_{max}, Rd and κ, respectively. The second curve -referred as 'saturated light response'- is taken from Collison et al. (2020) and the fitted parameters are 0.055, 30, 1.75 and 0.80. In this second curve, the saturation plateau is reached around 800 µmol m^{-2} s^{-1}.

2.4. Constructing CORNIBU digital canopies of actual maize canopies by estimating 3D model parameters from field measurements

Digital canopies of the five maize hybrids grown in the field experiment (see Section 2.1) were constructed using the CORNIBU model. To achieve that, the list of architectural model variables listed in Table 2 were estimated for the different GxR combinations based on the field measurements listed in previous Section.

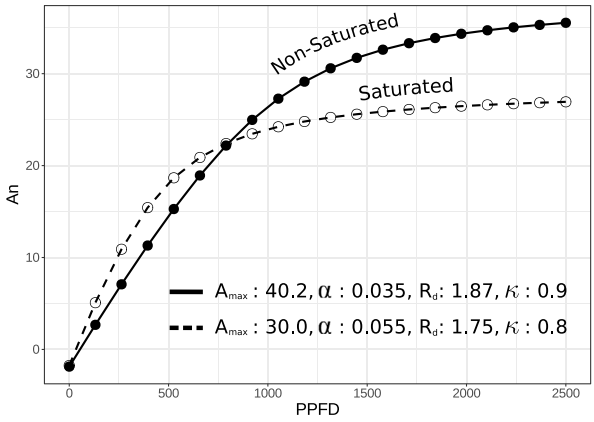

Fig. 3. Photosynthetic light–response curves scenarios of maize leaves exposed to different PPFD levels.

2.4.1. Estimation of leaves inclination parameters

The four parameters of leaf inclination $\theta_{i,top}$, $\theta_{i,base}$, $\Delta\theta_{base}$ and $L_{\Delta\theta}$ were determined from the leaf trajectories at the stage R1-R2 with the horizontal RGB images using the PoPCorn software (see Section 2.2.2 for further details).

To estimate all the four parameters for a given GxR combination -with a total of 18 plants-, the PoPCorn coordinates of all individual leaves trajectories in the plane (x, z) were extracted. For every leaf, the coordinate $(0, 0)$ represents the insertion point of the stem. The x and z coordinates refer respectively, to the horizontal and vertical distances from the insertion point. Leaves were then sorted depending on their position in the stem, from the top to the bottom of the plant. Then, a grid search algorithm was used to optimize all the four parameters together by minimizing the root mean squared error ($RMSE$) between the observed (PoPCorn coordinates) and estimated z-coordinates leaves trajectories (Vertical profile model Section 2.3.1), as:

$$RMSE(\theta_{i,top}, \theta_{i,base}, \Delta\theta_{base}, L_{\Delta\theta}) = \sqrt{\frac{\sum_l^n \sum_y^m \left[z(y,l) - z'(y,l,\theta_{i,top}, \theta_{i,base}, \Delta\theta_{base}, L_{\Delta\theta})\right]^2}{n \cdot m}} \tag{5}$$

where $z(y, l)$ is the observed z-coordinate in leaf l at the horizontal distance y from the insertion point, and z' is the simulated z-coordinate by the leaf inclination model with input variables l, $\theta_{i,top}$, $\theta_{i,base}$, $\Delta\theta_{base}$ and $L_{\Delta\theta}$.

2.4.2. Estimation of leaf dimensions and shape

As previously mentioned, the length and width relationship was taken from España et al. (1998). However, significant differences in such relationship were observed between our field measurements and those given by España et al. (1998) model. Therefore, we conducted an adjustment in the parameters : w_{max}, $i(l_{max})$ and l_{max} went from -0.0005i_t to -0.00065i_t, 0.31i_t to 0.27i_t and S_t to 0.94S_t, respectively.

2.4.3. Estimation of leaves orientation and phyllotaxy

The proposed maize architectural model is able to simulate leaf orientation using three input variables: ϕ_p and $\sigma_{\phi,p}$ are the parameters that describe the distribution of the plant azimuth in the canopy level, whereas $\sigma_{\phi,l}$ describe the variability of the azimuth for each individual leaf from the plant azimuth it belongs to.

Two alternative methods to derive the leaves orientation parameters were evaluated. The ALAEM algorithm (Serouart et al., 2023) permitted to retrieve a distribution of the leaves orientation relative to the rows, at the canopy scale. However, it is also important to quantify how much the dispersion (around the most frequent orientation) comes from the phyllotaxy ($\sigma_{\phi,l}$) and from the variability of plant orientation ($\sigma_{\phi,p}$),

since the two variables play a different role in determining mutual shading at the plant and canopy scale.

In the first method (called 'Measured Phyllotaxy'), the phyllotaxy parameter $\sigma_{\phi,l}$ were taken from a manual phyllotaxy measurements done at R1-R2 stage for the 18 (6 × 3 blocks) plants per GxR combination sampled destructively to determine leaf trajectories (Section 2.2.2). Once phyllotaxy was fixed, the parameters for plant distribution were optimized. To achieve that, a probability distribution was fitted to the histogram of observed leaves orientation by minimizing the sum of squared errors (SSE) between the observed and estimated frequencies. A wide panel (~105) of theoretical probability distributions from the scipy.stats package (SciPy, 2020) were fitted to the data. The distribution of the one providing the lowest SSE was finally selected. If the chosen distribution is different from the normal distribution, the parameters for plant orientation distribution ϕ_p and $\sigma_{\phi,p}$ are replaced by those of the chosen distribution.

The second approach (called 'Derived Phyllotaxy'), uses observed gap fraction measurements in the zenith direction (Section 2.2.4) to estimate $\sigma_{\phi,l}$. The purpose of this second method is to circumvent the possible representativeness uncertainties of the manual phyllotaxy measurements, acquired in a reduced number of plants per GxR treatment. Basically, the Derived Phyllotaxy method consists of decomposing the overall standard deviation of the leaves azimuth at the canopy level provided by the ALAEM method into $\sigma_{\phi,p}$ and $\sigma_{\phi,l}$. The architectural maize model assumes that both, plant orientation and phyllotaxy follow a normal distribution, and therefore:

$$\sigma_{\phi,c} = \sigma_{\phi,p} + \sigma_{\phi,l} \tag{6}$$

where $\sigma_{\phi,c}$ is the observed standard deviation of leaves orientation at the canopy level provided by ALAEM. When the ratio $\sigma_{\phi,p}/\sigma_{\phi,l}$ is equal to 0, it means that all the variance at the canopy level is explained by phyllotaxy (i.e. all the plants in the canopy are oriented exactly the same). Conversely, when $\sigma_{\phi,p}/\sigma_{\phi,l} = 1$ all the variance at the canopy level is explained by the variance of plant orientation, meaning that all leaves in the plant follow a perfect distichous phyllotaxy, with all leaves distributed in the same horizontal axis.

To decompose the observed variance into $\sigma_{\phi,p}$ and $\sigma_{\phi,l}$ for every GxR combination, the ratio $\sigma_{\phi,p}/\sigma_{\phi,l}$ is optimized by minimizing numerically the difference between the gap fraction at zenith view measured from hemispherical photographs (Section 2.2.4) and simulated from the maize architectural model, by fixing all the other architectural variables to the previously estimated values for each maize hybrid. The method followed to derive canopy gap fraction from the digital canopies is presented in the next Section 2.4.4.

2.4.4. Validating digital canopies from canopy gap fraction measurements

For every digital canopy of the architecture model, 10 replicates of 3D maize scenes at development stage R1-R2 were generated with the set of input variables estimated for each GxR combination. On each 3D scene, 50 digital hemispherical photographs were simulated using the POVRay ray-tracing software (POVRay, Persistence of Vision Pty. Ltd. (2013)) following the same optical configuration and spatial sampling as field measurement (Section 2.2.4). Then, canopy gap fraction at different viewing directions $P_0(\theta_t, \phi_t)$ was computed from the simulated/digital hemispherical photographs.

The computed digital canopies for every GxR combination were evaluated by comparing the gap fraction observed in the field against the simulated ones, according to the two mentionned methods to derive leaves phyllotaxy ('Measured' and 'Derived Phyllotaxy'). Moreover, daily $fIPAR$ is computed from the directional gap fractions retrieved in the hemispherical images by integrating 1-P_0 using the sun position in the Montardon site, at the date of the field measurements:

$$fIPAR_d = \frac{\sum_{t=0}^{n} \left[1 - P_0(\theta_t, \phi_t)\right] \cdot \cos\theta_t}{\sum_{t=0}^{n} \cos\theta_t} \tag{7}$$

where θ_t and ϕ_t are the sun zenith and azimuth angles at time t between sunrise and sunset. The gap fraction above 60° angles θ_t were extrapolated using Beer–Lambert law, as proposed in the CAN-EYE model (https://www.paca.inrae.fr/can-eye/Documentation/Documentation) to compute daily $fIPAR$. This comparison between gap fraction and daily $fIPAR$ permits to assess the reliability of the architectural model proposed to simulate the actual light interception of the five maize hybrids, studied under different sowing patterns.

2.5. Construction of an in silico experiment with CORNIBU to identify maize ideotypes for light interception and optimal sowing patterns

The CORNIBU model was used to design an *in silico* experiment by varying the input architectural variables listed in Table 2 within the proposed intervals. To explore the variables space randomly and efficiently, the Latin Hypercube Sampling strategy (LHS, Tang, 1993) was used to generate a total of 5500 three-dimensional scenes using the lhs (Carnell, 2022) package in R. This sampling strategy ensures unbiased scanning of all possible inputs combinations -the phenotypic space-. The total of 5500 scenes resulted in 50 × 110 stand and plant architectures, respectively. The exact procedure is described below.

The distribution of the sampling combinations -of input variables derived from LHS- is given in Fig. 4. On this Figure, the left panel (a) describes the sampling distribution of the 50 stand architecture combinations, each point is a $D \times S_{max} \times dr$ combination. The exact same scheme is applied on the right panel (b), where each point is a plant architecture combination, 110 in total (by varying $\theta_{i,base}$, $\theta_{i,top}$, $\Delta\theta_{base}$, $L_{\Delta\theta}$, ϕ_p, $\sigma_{\phi,p}$ and $\sigma_{\phi,l}$). By combining the two panels, it resulted in 5500 combinations of 3D scenes used in the *in silico* experiment. The scenes were generated for the R1-R2 development stage, when plant leaf area is fully expanded.

To sample accurately plant density D, leaf area per plant S_{max} and row spacing dr, the actual in field experiment relationship observed between D and S_{max} was used to define a parallelepiped interval -between both variables- (Fig. 4). This strategy prevents from unrealistic situations, where leaf area per plant is large under high plant density (>10 plants m^{-2}), which may bias the choice of the ideotypes, while guaranteeing a reasonable leaf area index. The distance between rows (dr) was sampled uniformly. A total of 50 $D \times S_{max} \times dr$ combinations were sampled. For the other seven architectural variables ($\theta_{i,base}$, $\theta_{i,top}$, $\Delta\theta_{base}$ and $L_{\Delta\theta}$ for leaves inclination and curvature; ϕ_p, $\sigma_{\phi,p}$ and $\sigma_{\phi,l}$ for leaves orientation), 110 combinations were drawn randomly following the LHS. The product between the two samplings results in the total of 5500 simulated scenes.

Over the total set of 5500 scenes, Caribu was used to compute $fIPAR$ and $fILA$ under direct and diffuse conditions. Daily canopy photosynthesis A_d was also considered, as explained in Section 2.3.2. The variability of $fIPAR$, $fILA$ and A_d across the set of 5500 was analyzed. The ideotype and the optimal sowing pattern are, theoretically, the combination that yields the highest $fIPAR$, $fILA$ and consequently, A_d. When analyzing the impact of the architectural variables in daily canopy photosynthesis along Section 3, A_d will be expressed in relative units: A_n relative to the median value across the canopies simulated.

Additionally, a sensitivity analysis was conducted over the virtual scenes to quantify the sensitivity of $fIPAR$ and $fILA$ to the different maize architectural parameters. For this, a polynomial linear metamodel (plmm) of an order of 2 (bilinear) was conducted over the set of leaves inclination and orientation variables, including interaction terms. To reduce the dimensionality of the plmm, the leaf inclination variables $\theta_{i,base}$, $\theta_{i,top}$, $\Delta\theta_{base}$ and $L_{\Delta\theta}$ were integrated into a single variable by computing the average leaf angle (ALA) of the plant from each combination of those four variables. The ALA takes the value of 0° for erected leaves and 90° for horizontal leaves. An individual plmm is applied for every $D \times S_{max} \times dr$ combination.

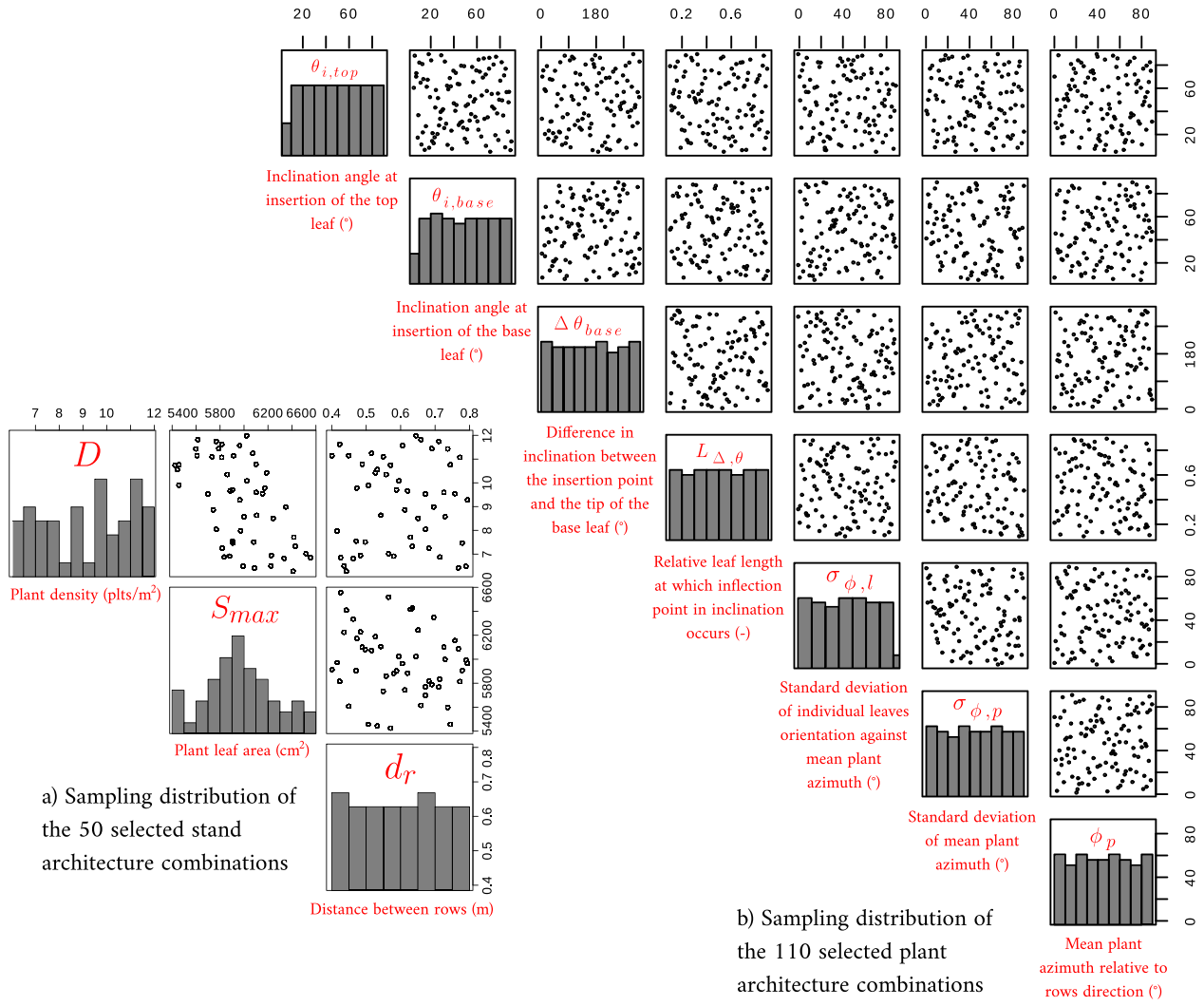

Fig. 4. Pairwise (2-by-2) scatter plots of the LHS sampling distribution of input variables. This LHS sampling was used to generate the CORNIBU *in silico* experiment and ensure that we had sufficiently explore the phenotypic space. The left panel (a) describes the sampling distribution of the 50 selected stand architecture combinations -each point is a $D \times S_{max} \times dr$ combination-. The exact same scheme is applied on right panel (b). Each point is a plant architecture combination, among the 110 selected (by varying $\theta_{i,base}$, $\theta_{i,top}$, $\Delta\theta_{base}$, $L_{\Delta\theta}$, ϕ_p, $\sigma_{\phi,p}$ and $\sigma_{\phi,l}$). By combining the two panels, it resulted to 5500 combinations of 3D scenes available for the *in silico* experiment. Note that D, S_{max} and dr (the left panel (a), 50 samples) were sampled separately to avoid unrealistic combinations of D and S_{max}, e.g. large leaf area per plant under high plant density.

The plmm and the sensitivity indices were computed using the R packages mtk and plmm (Wang et al., 2015; Faivre et al., 2013). These indices assess the percentage of variance in $fIPAR$ and $fILA$ that can be elucidated by each of the four parameters studied in comparison to the overall variance. The stepwise model selection method (stepAIC) was applied to identify the optimal models. Finally, to compute canopy-level photoynthesis we used $QPAR$ and fd hourly data measured by the INRAE agro-meteorological weather station at the Avignon site (43° 54′59″N, 4° 52′43″E) in July 2023.

3. Results

3.1. Accuracy of CORNIBU digital canopies to simulate the architectural parameters of actual maize hybrids

3.1.1. Individual leaf dimensions

In the proposed architecture model, the width and length of each leaf are modeled applying the allometric equations proposed by España et al. (1998), that take N_{max} and S_{max} as input parameters. The comparison between the leaf dimensions predicted by these allometric equations and those observed from manual measurements knowing N_{max} and S_{max} are shown in Fig. 5.

The leaves lengths predicted by the architecture model exhibited a high accuracy, with an average error of approximately 6.5 cm (Fig. 5a–d). In the R1, R2 and R4 patterns no substantial bias is observed, whereas the R8 displayed a slight underestimation for the longest leaves (>85 cm). Such longer leaves behavior may be promoted by a photomorphogenetic response to neighbors in high plant density patterns, which was not considered by the model. In all the four rectangularity treatments, the predicted length of individual leaves is strongly correlated with the observed values across leaf orders and maize hybrids ($R^2 > 0.92$).

The errors in individual leaf width are below 1 cm on average (Fig. 5e–h), with a negligible bias in all the four rectangularity patterns. Similarly, the correlation between observed and modeled leaves width for each sowing pattern indicates that model predictions describe more than 91% of the variability across leaf orders and hybrids.

3.1.2. Leaves orientation and inclination

The architectural variables describing leaf orientation were estimated using the two approaches described in Section 2.4.3. Fig. 6a shows the observed and modeled leaves orientation distribution for the IGNATIUS hybrid in the R8 treatment from raw ALAEM data (Serouart et al., 2023, Fig. S1). The distributions for all GxR combinations are

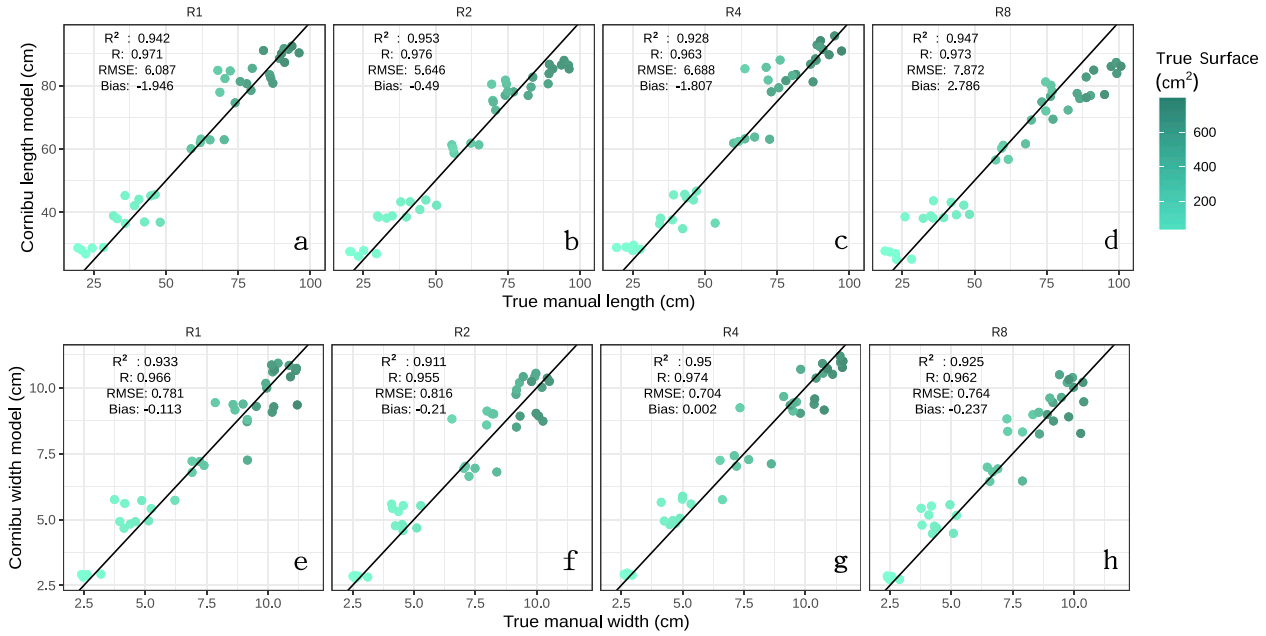

Fig. 5. Accuracy of the 3D maize architecture model predictions of individual leaves length (top) and width (bottom) for the sowing patterns R1, R2, R4 and R8. Each scatter plot includes leaves at different stem positions measured in situ for the five maize hybrids studied.

given in Figure S3. In Fig. 7 and S5, the strategy assuming that the variable $\sigma_{\phi,l}$ (standard deviation of individual leaf orientation) known from manual measurements provides, overall, a better agreement against the observed leaf orientation distributions when compared with the strategy where the ratio between $\sigma_{\phi,l}$ and $\sigma_{\phi,p}$ is optimized from vertical gap fraction measurements. In the first strategy, the choice of the distribution among a wide range of theoretical distributions permits to maximize the fit to the empirical distribution observed from ALAEM in the field. In the second strategy, the retrieved values of $\sigma_{\phi,l}$ are systematically higher as compared to the manual measurements over a reduced number of plants. According to this, manual measurements indicates that plants tend to follow an almost perfect distichous phyllotaxy, whereas the optimization of $\sigma_{\phi,l}$ from gap fraction values suggest that leaves have a moderate deviation -between 10° and 20°- from the main plant axis.

The optimization of the leaf inclination and curvature parameters, from the profile plant images, produced an uncertainty of 7.5 cm in the midrib positions between observed and modeled leaf trajectories, which is considered as satisfactory. Fig. 6b also depicts the observed and modeled leaves trajectories of the IGNATIUS hybrid under the R8 sowing pattern. The trajectories for all GxR combinations are given in Figure S4. As it can be appreciated, the set of parameters optimized for the different varieties is able to describe properly the main differences on leaves inclination and curvature between the five hybrids studied. The inclination variables $\theta_{i,base}$ and $\Delta\theta_{base}$ are those presenting the highest differences among the hybrids, with MONTAG and DANTES hybrids presenting a higher leaves curvature compared to all others (Figure S4).

3.2. Reliability of CORNIBU digital canopies to describe the gap fraction of actual maize hybrid canopies under different sowing patterns

The relationship between the observed and simulated gap fraction per zenith angle for all the four sowing patterns is given in Fig. 7. The R2 pattern (12 plants m^{-2}, 0.4 m row spacing) systematically intercepts more radiation in both, digital canopies and actual canopies. In general, at zenith angles that depart from zenith (i.e. between 15° and 45°) the observed and modeled gap fraction from the digital canopies agree.

By contrast, the differences between the observed and modeled gap fraction are more important in angles close to zenith (<10°), where light interception is lower and the role of some architectural variables -such as leaf inclination and leaves orientation- is important. At these low zenith angles, deriving the ratio $\sigma_{\phi,p}/\sigma_{\phi,l}$ from gap fraction measurements (Fig. 7, bottom) improves significantly the reliability of the maize model to describe light interception as compared to measuring directly manually leaf over a small number of plants (Fig. 7, top). Such improvement is particularly important in the low rectangularity patterns R1 and R2. However, in such R4 and R8 patterns, it is only clearly appreciable for certain hybrids (DANTES and ESMERALDA in R4, WINSTON in R8).

The reliability of the digital canopies to describe actual gap fraction also depends on the considered hybrid. In almost all the four sowing patterns, a slight, but systematic underestimation -at zenith angles higher than 15°- is observed for the MONTAG hybrid (e.g. treatment R8, Fig. 7, top and bottom). In the R4 treatment, WINSTON cultivar digital canopy exhibits a substantially higher gap fraction compared to the observed one from hemispherical images. However, in all the other three patterns, both digital canopy and the actual hybrid agree.

The relationship between the observed and simulated gap fraction per genotypes for all the four sowing patterns is also given in Figure S5.

These results are corroborated by Fig. 8, where the accuracy of the daily $fIPAR$ estimation from 'Derived Phyllotaxy' -method of phyllotaxy optimization by gap fraction- is significantly higher than from ground manual measurements -based on 10 plants sample- (R^2 ~ 0.6 vs. 0.27, respectively).

3.3. Contribution of maize plant architectural traits to light interception, light distribution and canopy photosynthesis

3.3.1. Sensitivity analysis of fIPAR, fILA to plant inclination and orientation

Leaf inclination is the architectural variable that has the largest influence on both, $fIPAR$ and $fILA$, as displayed in Fig. 9 and Tables ST2-ST3, which list the explicit values of each trait contribution. The variable ALA, which integrates the information about leaves inclination and curvature along the vertical plant profile is responsible for 85% and 75% of the $fILA$ and $fIPAR$ variance, respectively. This large preeminence of the ALA as the main factor explaining light interception

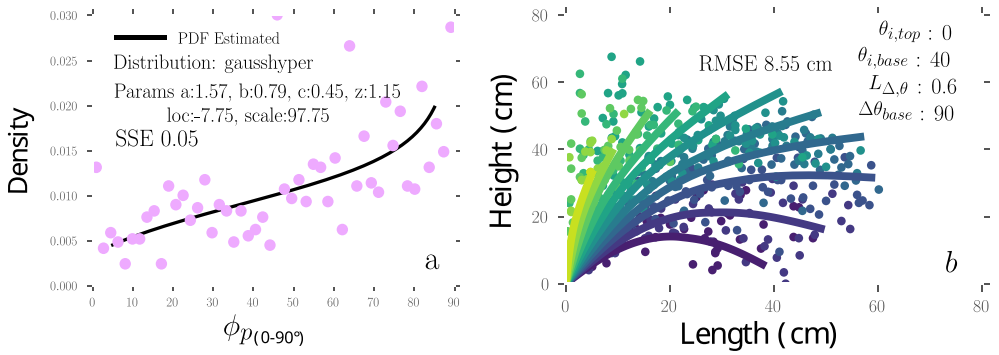

Fig. 6. a. Fitted azimuthal probability distribution functions to empirical data with Measured phyllotaxy approach b. Fitted elevation function to empirical data. Both graphs belong to the IGNATIUS hybrid and the R8 sowing pattern. The results obtained for the other sowing patterns and hybrids are given in supplementary material S3 figure.

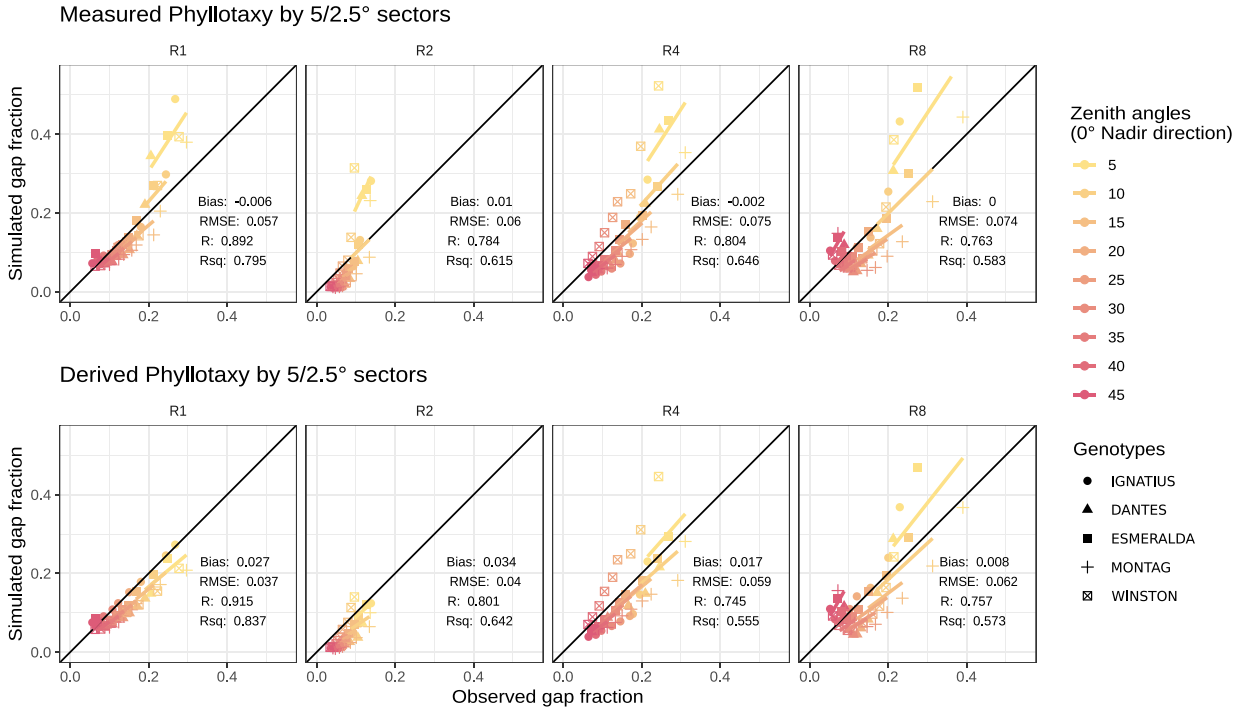

Fig. 7. Relationship between the observed gap fraction in actual maize hybrid canopies at different zenith angles and sowing patterns and the gap fraction simulated from the CORNIBU digital canopies. The top row the phyllotaxy of the digital canopies was established from manual in situ measurements, whereas in the bottom row leaf phyllotaxy parameters were derived from observed gap fraction. The maize development stage was R1-R2.

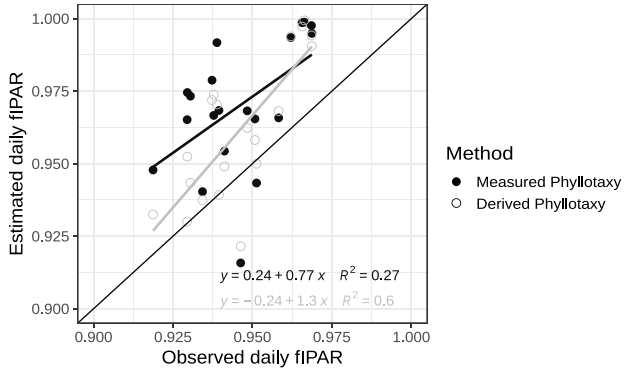

Fig. 8. Difference between observed and estimated daily fIPAR. The measured fIPAR was obtained in the field across 20 treatments (5 hybrids × 4 Rectangularity levels) using the DHP method. The simulated fIPAR was generated using CORNIBU over the same 20 treatments. Two approaches were employed to characterize azimuthal conditions, with the phyllotaxy parameter being either manually measured or derived from in situ gap fraction measurements.

and light distribution is systematic, regardless of the considered sowing patterns and the total leaf area per plant.

The variance of $fIPAR$ explained by leaf orientation parameters is about 25%, the standard deviation of the plant azimuth $\sigma_{\phi,p}$, which controls the possible overlap between plants within the same row, is the most important factor. Both, the mean plant azimuth ϕ_p and the phyllotaxy variable $\sigma_{\phi,l}$ seem to have a minor importance in determining $fIPAR$.

Accuracy of Sensitivity Analysis polynomial models for Direct and Diffuse conditions may be found in Figure S6 and S7, respectively.

3.3.2. Optimal architectural traits for light interception, distribution and canopy photosynthesis

The analysis of $fIPAR$ and $fILA$ computed over the 5500 scenes of the experimental plant permitted to identify the architectural parameters that maximized both light regime variables. The architectural variables that maximize $fIPAR$ and $fILA$ are relatively similar at different densities and row spacing distances.

As described in Fig. 10 a, the architectural traits that provided the highest light interception (highest $fIPAR$) are planophile (leave

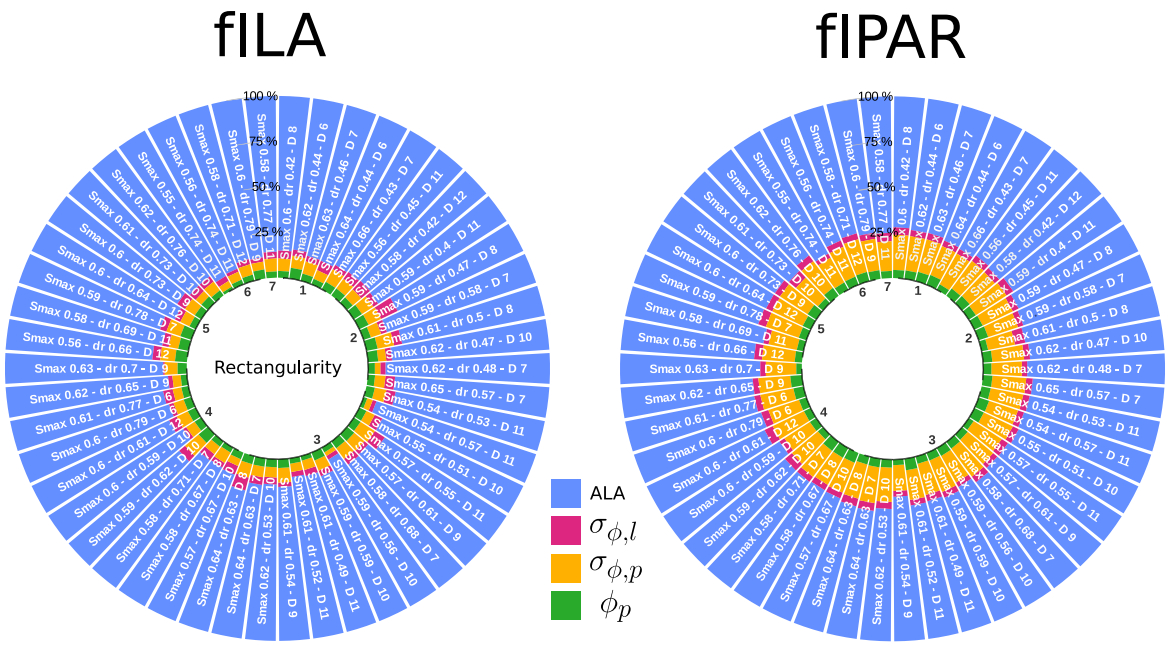

Fig. 9. Variance of fILA and fIPAR under direct light conditions explained by the different leaf inclination (ALA) and leaf orientation parameters (ϕ_p, $\sigma_{\phi,p}$ and $\sigma_{\phi,l}$) for every combination of plant density (D), distance between rows (dr) and plant leaf area (S_{max}). The numbers in the inner circles of the graph refer to the rectangularity of the sowing pattern.

inclination distributions with ALA ~ 80°) and with a large variance in plant and leaves orientations in the stand ($\sigma_{\phi,p}$ and $\sigma_{\phi,l}$ ranging between 73° and 87°).

By contrast, maximizing incoming light distribution ($fILA$) within the foliage requires, essentially, erectophile leaves (Fig. 10b) with an average leaf angle around 25 degrees and top leaves always more inclined than bottom ones ($\theta_{i,top} < \theta_{i,base}$). Regarding leaf orientation, the mean plant azimuth (ϕ_p) that maximize $fILA$ is around 45–50° relative to the row direction, with a small variability of plant orientation at the canopy level ($\sigma_{\phi,p}$ ~ 20°) and a moderate variability of leaves orientation within the same plant ($\sigma_{\phi,l}$ ~ 40°). This set of architectural parameters permit to reduce mutual shading at both, plant and canopy scales, but at the cost of intercepting a smaller proportion of incoming light, especially at nadir directions (Fig. 10b).

This dichotomy between light interception and distribution at the canopy scale is illustrated in Fig. 11, which shows all the 5500 3D scenes of the *in silico* experiment -each point is a scene-. On the left panel is considered only the Non-Saturated photosynthetic light response curve scenario, on the right the Saturated curve. The colors describe A_n, the daily canopy-level photosynthesis. The points colored in red bold highlight the canopies with the highest A_n (top 5% scenes) for each panel/light curve scenario. It can be seen a clear relationship between canopy $fIPAR$ and $fILA$. Indeed, the photosynthetic light response curves do not maximize the same metric -$fIPAR$ vs. $fILA$- and it is not possible to maximize both at the same time; there is a trade-off involved. A good light distribution cannot occur simultaneously with an optimal light interception, as clearly visible through Fig. 11. The stand/maize architectural combinations -among 5500- that maximize $fIPAR$ (0.96) produce a decrease in the amount of leaf area that is actually illuminated (0.911). The decrease of $fILA$ is more pronounced as $fIPAR$ approaches to 1. And reciprocally on the right panel, an increase of $fILA$ (0.971) always leads to a decrease of the amount of light that is actually intercepted by leaves (0.92). These results indicate a trade-off between light interception and light distribution due to mutual shading.

On the other hand, the non-saturated and saturated light-response curves yielded two contrasted architectural ideotypes on what regards canopy-level photosynthesis. Under non-saturated light-response, the ideotype that produce the highest canopy-level photosynthesis coincides with the architecture that maximizes the $fIPAR$ (Figs. 10, 12): flat and planophile leaves with an almost random leaves orientation.

By contrast, under the saturated light-response curve, the selected ideotype privileges $fILA$ over $fIPAR$, as shown in Figs. 10 and 12: inclined and curved leaves (ALA 40°, $\Delta\theta_{base}$ 78°) with a progressive increase in the leaves inclination from the bottom towards the upper leaves. Thanks to this progressive vertical distribution of leaves inclination, light interception by the middle and bottom leaves is enhanced. Regarding leaves orientation, the ideotype based on the saturated light-response curves presents a preferred leaves orientation close to 50°, with a small variance both at the canopy ($\sigma_{\phi,p}$) and plant scale ($\sigma_{\phi,l}$), thus avoiding an excessive mutual shading between different plants.

3.4. Effect of plant density and row spacing in fIPAR, fILA and canopy photosynthesis

Fig. 13 shows the variability of daily canopy photosynthesis, $fIPAR$ and $fILA$, respectively rows 1, 2 and 3. Each panel depending on the density (y-axis) and the sowing pattern (Rectangularity, x-axis). Finally, the two plant architecture ideotypes -through Saturated and Non-Saturated light-response curves- are represented respectively on columns 1 and 2.

Overall, for both ideotypes, increasing plant density will produce an augmentation of $fIPAR$ and a reduction of $fILA$, reciprocally when plant density decreases -Fig. 13(c) vs. (e) and Fig. 13(d) vs. (f)-. For the erectophile ideotpype, determined from the saturated light-response curve, a low rectangularity pattern (R, x-axis) has a positive effect on both $fIPAR$ (Fig. 13c) and $fILA$ (Fig. 13e), whatever the density considered. By contrast plant rectangularity does not have a substantial effect on $fIPAR$ for the planophile ideotype (non-saturated light-response, Fig. 13d), whereas $fILA$ increases when rectangularity is lower than 4 (Fig. 13f).

Similarly, the relationship between the sowing pattern (R, x-axis) and A_n varies also depending on the linearity of the light-response curve and the resulting ideotypes (Fig. 13a, b). In the non-saturated

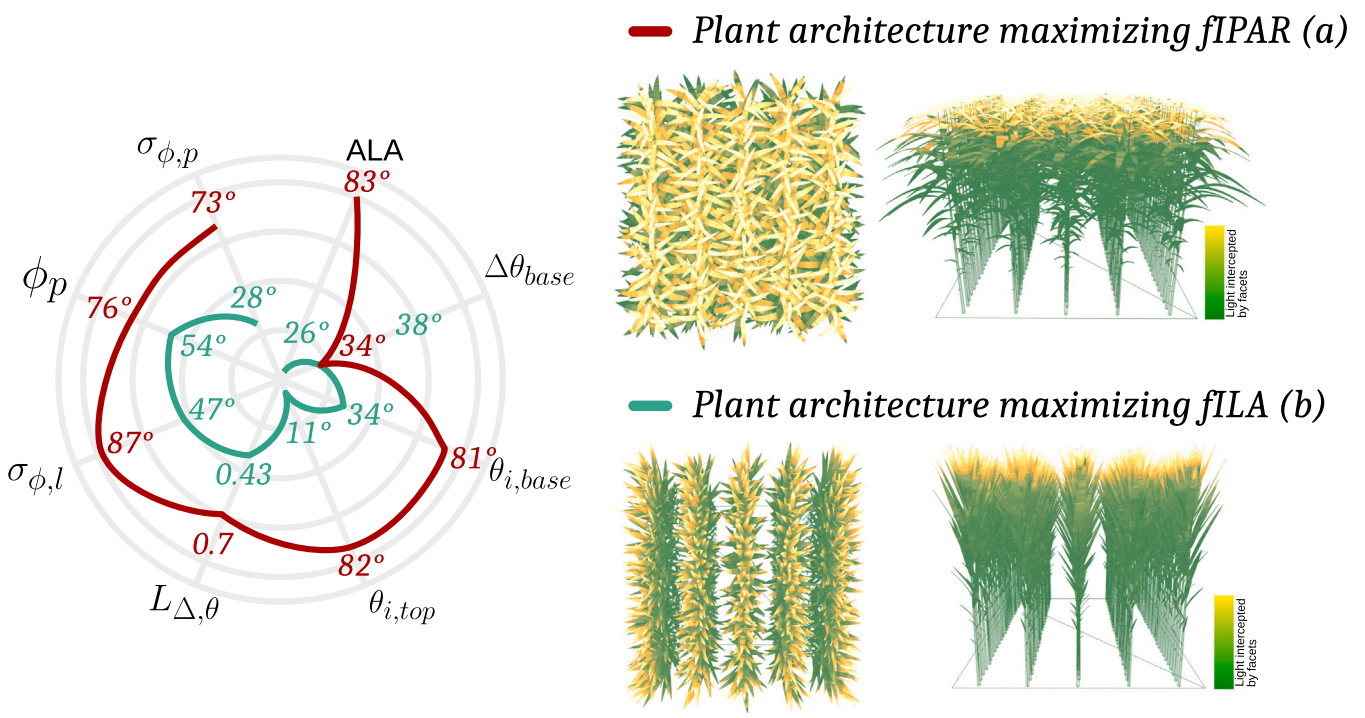

Fig. 10. Maize architectural variables of the 3D maize model of the ideotypes identified through the in silico analysis that maximize light interception (fIPAR, in red) and light distribution (fILA, green) for a single sowing density pattern, here R8. a,b: vertical and horizontal views of the fIPAR and fILA ideotypes.

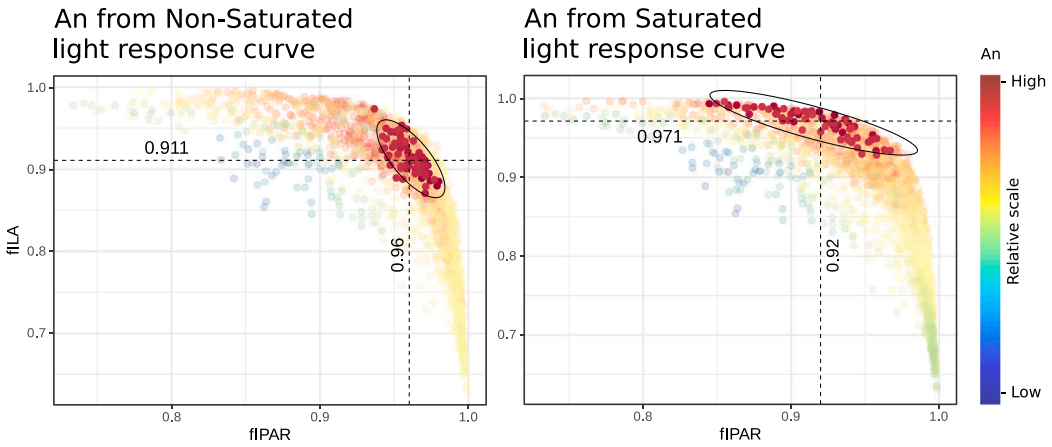

Fig. 11. Trade-off between light interception and distribution at the canopy scale. Here is represented the relationship between canopy $fIPAR$ and $fILA$ under the two studied photosynthetic light response curve scenarios for the 5500 maize 3D scenes created in the *in silico* experiment. On the left panel is considered only the Non-Saturated photosynthetic light response curve, on the right the Saturated curve. The colors describe A_n, the daily canopy-level photosynthesis. The points colored in red bold highlight the canopies with the highest A_n (top 5% scenes) for each panel/light curve scenario.

light response, the highest photosynthesis is achieved at low rectangularity and low plant density (Fig. 13b). Since the planophile ideotype identified for this response curve relies on maximizing $fIPAR$ (Fig. 13d), increasing plant density and rectangularity exacerbates mutual shading, resulting in lower photosynthesis rates as compared to low density patterns (Fig. 13b). By contrast, in the saturated light response scenario (Fig. 13a), the highest photosynthesis rates are achieved at high density (9–10 plants m-2) and low rectangularity (R around 1 or 2, corresponding to a row spacing of about 0.4 m). Since the architectural ideotype for this scenario has more inclined leaves (Fig. 12) to improve light distribution, mutual shading is not large enough to have a negative impact in canopy photosynthesis at a relatively high plant density in a square sowing pattern.

4. Discussion

4.1. Reliability of CORNIBU to model maize light interception

The digital canopies of the five maize hybrids simulated with CORNIBU described satisfactorily the variability of daily $fIPAR$ observed in the field over different sowing pattern levels (R^2 of 0.6 for the 'Phyllotaxy Derived' method). For that reason, we consider that CORNIBU, if the architectural parameters are adequately set, can be used to predict canopy light interception in maize. To our knowledge, the previous works proposing architectural maize models did not assess the ability to predict fIPAR on actual field experiments.

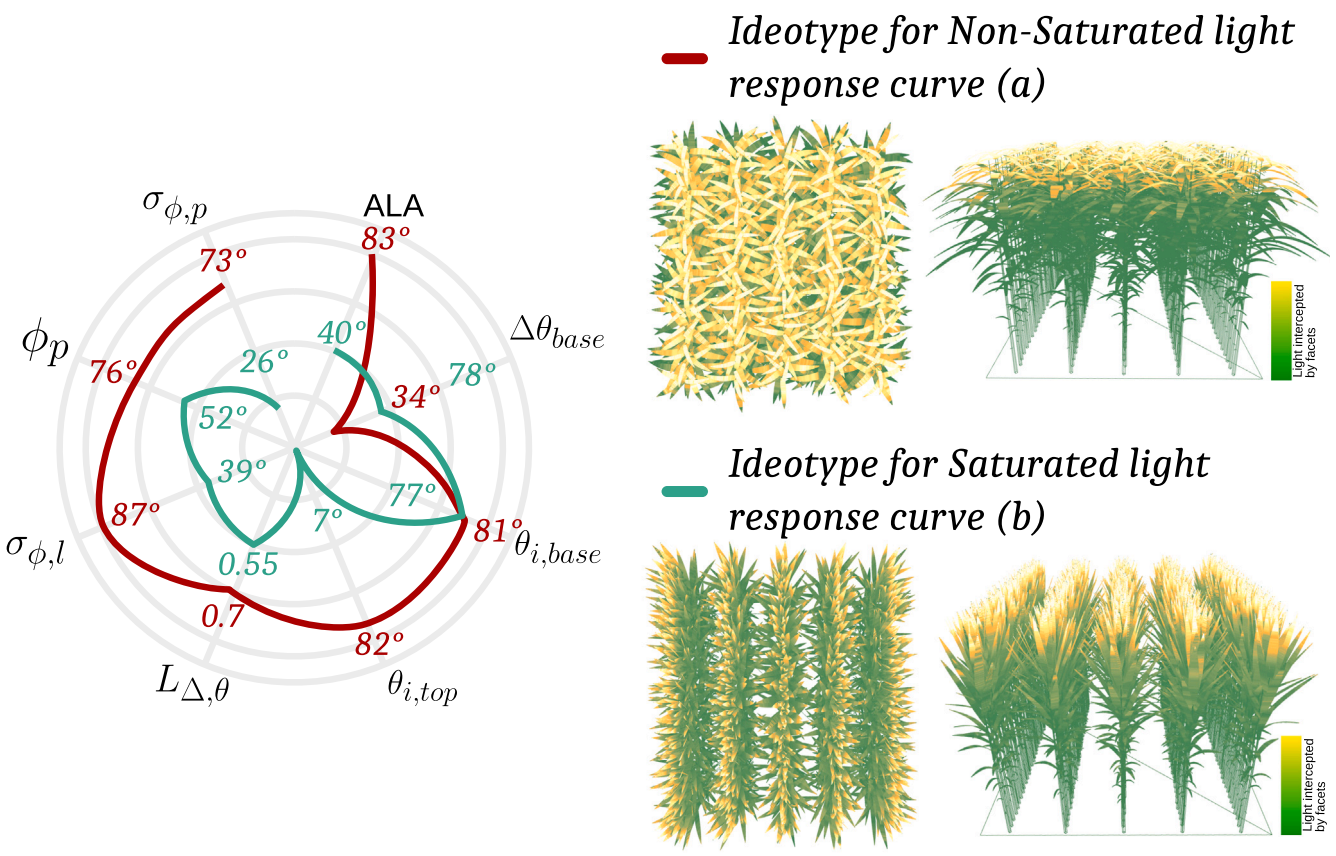

Fig. 12. Maize ideotypes yielding the highest daily canopy photosynthesis A_d from the in silico experiment for non-saturated and saturated light-response curves. The panel on left-side shows the value of the architectural variables and the panel on right-side provides a vertical and horizontal view of the A_d ideotypes 3D canopies.

Our results indicate that the method followed to set the values of leaves orientation (particularly variables $\sigma_{\phi,p}$ and $\sigma_{\phi,l}$) is highly relevant since orientation has an important contribution to $fIPAR$. While manual measurements of leaves orientation in individual plants are time-consuming and often not representative of a given plot (Serouart et al., 2023), the ALAEM method based on RGB images proved to be efficient in providing a realistic distribution of leaves orientation at the canopy scale. However, ALAEM does not provide an explicit description of leaf phyllotaxy, which is a crucial aspect since it controls the arrangement and overlap between leaves on the same plant. The 'Derived Phyllotaxy' approach introduced in this paper, involving the numerical optimization of the ratio $\sigma_{\phi,p}/\sigma_{\phi,l}$ using nadir gap fraction observations, helped to improve the reliability of the modeled gap fraction and extended $fIPAR$. Since ALAEM uses vertical images for computing leaf orientation distribution, the identical set of images can also be used to derive plant phyllotaxy and, at the same time, improving the reliability of the architectural model to predict $fIPAR$ also in directions far from nadir (Fig. 7), obviously once all the other architectural variables are known.

The model formalisms adopted to describe leaves inclination (from Perez et al., 2016) yielded a vertical positioning error of 7.5 cm along the entire trajectory. This is considered acceptable since the variability of leaves inclination and curvature across the five maize hybrids observed in the field is, overall, well described (Figure S4). Our intent to maintain a simple model and consider the entire inclination dynamics with only four parameters involves rigid assumptions, particularly in the variability of inclination and curvature depending of leaves rank. These assumptions introduce, necessarily, some errors in the actual leaves trajectories, but permitted to explore easily the phenotypic space range in the *in silico* experiment.

The proposed architectural model does not simulate the continuous leaf expansion through a linear response curve to temperature but rather provides a static description of the canopy at a given leaf number stage. Implementing a continuous function to simulate leaf expansion from temperature would be relatively straightforward, however, describing the dynamics of leaves inclination and curvature depending from leaf age (as a classical FSPM would) requires much more complex model formalisms. Furthermore, the model does not simulate explicitly architectural plasticity or photomorphogenesis. This represents a significant limitation for applications that would require to simulate changes in leaf inclination and, particularly, leaf orientation over time in response to the local environment. The mechanisms of plasticity in these aspects are not fully understood at this point.

In the current study we determined the traits describing leaves inclination and curvature from the manual digitalization of plant silhouettes. Manual measurements restrict the number of plants that could be sampled per genotype and sowing pattern, impacting negatively the representativeness of the retrieved values for these parameters. In this context, the analysis of dense 3D point clouds, either provided by terrestrial LiDAR devices (Light Detection And Ranging), either generated from multi-view RGB imagery, can provide high-throughput and non-destructive measurements of several plant architectural variables (Su et al., 2019; Xiao et al., 2023; Jin et al., 2018a,b). In dense canopies, occlusions between plant organs are frequent, and they constitute a challenge to re-construct explicitly the plant organs from 3D point clouds. However, point clouds can provide an accurate description at least of the top canopy layer, where occlusions are less common. Analyzing the dynamics of the top canopy layers with frequent LIDAR or UAV acquisitions constitutes a promising way to achieve a complete description of plant architecture.

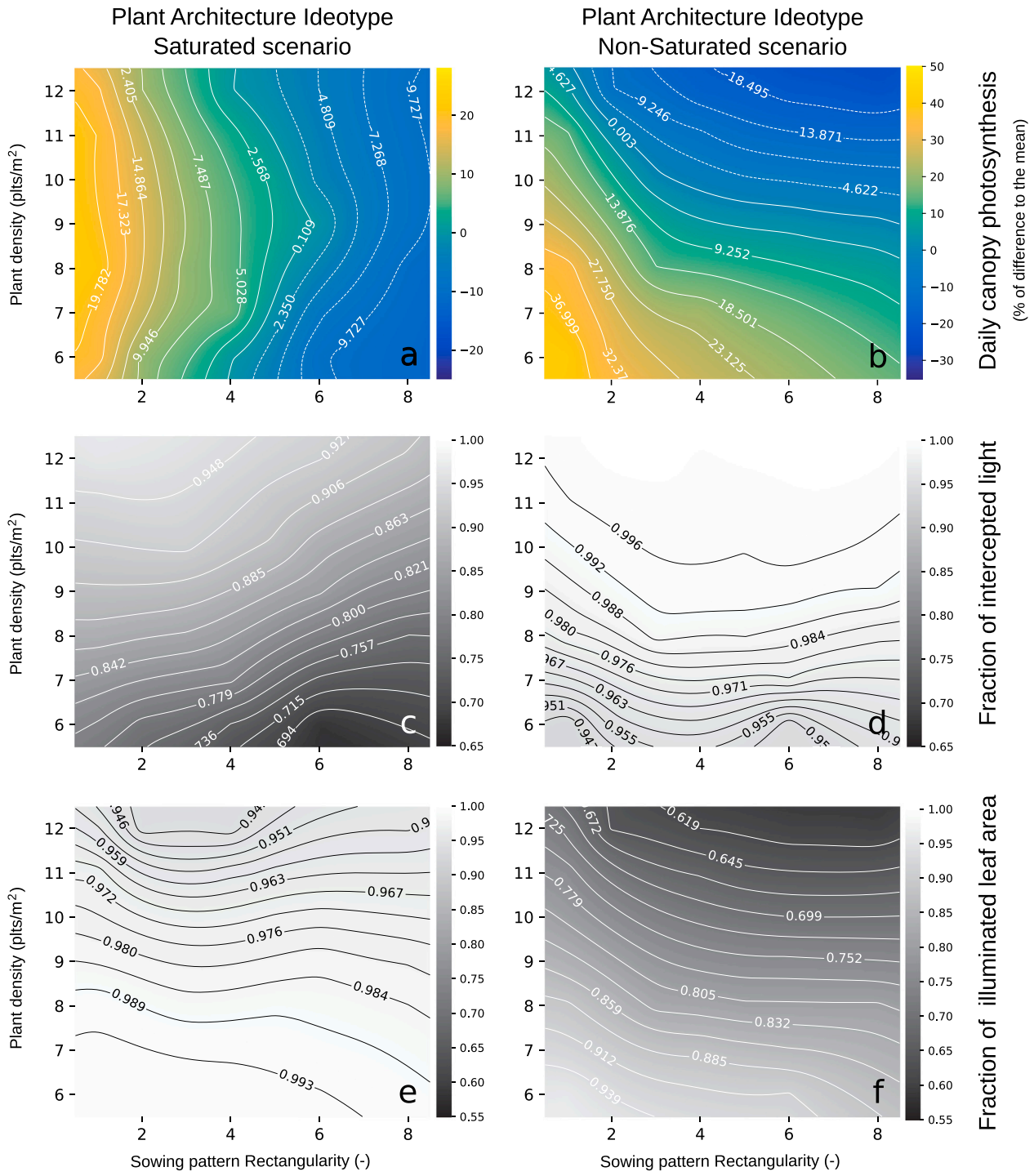

Fig. 13. Variability of daily canopy photosynthesis, $fIPAR$ and $fILA$ -respectively row 1, 2 and 3-. All the panel depending on the density (on y-axis) and on the sowing pattern (Rectangularity, x-axis). The two ideotypes defined from the Saturated and Non-Saturated photosynthetic light-response curves scenario are depicted on column 1 and 2, respectively. On the first row (panel a and b), An for a given $D \times dr$ is expressed as the relative difference (in %) against the mean daily canopy photosynthesis across all the $D \times dr$ combinations.

4.2. Light interception vs. light distribution in determining canopy photosynthesis: What is the best plant architecture ?

The results presented in Section 3.3.2 revealed a clear trade-off between light interception ($fIPAR$) and light distribution ($fILA$) in closed maize canopies, so any architecture cannot maximize both at the same time (Fig. 11). The optimal balance between $fIPAR$ and $fILA$ that permits to increase photosynthesis at the canopy scale -in other words, the architectural ideotype- is determined by the curvature of the light-response function at the leaf level. Fig. 14 shows the distribution of light intensity (absorbed PPFD) per facet in the 3D scenes ideotypes identified assuming the non-saturated and saturated light-response curves. To maximize canopy-level photosynthesis, leaf area must be distributed in those intervals of the light-response curve with a higher 1st derivative. When the light-response curve is almost linear (non-saturated) the ideotype that maximizes canopy-photosynthesis has a relatively stable proportion of leaf area at PPFD >50 μmol m^{-2} s^{-1}, increasing moderately at PPFD >750 μmol m^{-2} s^{-1}. By contrast, under a

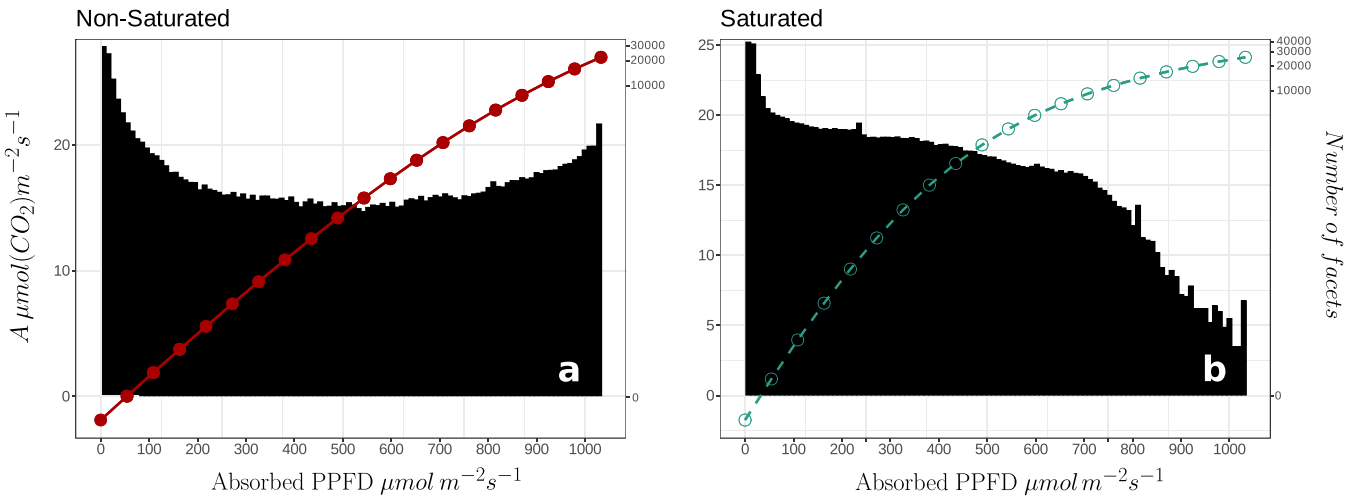

Fig. 14. Distribution of the simulated absorbed PPFD at 12:00 solar time per facet in the 3D scenes of ideotypes identified from the non-saturated (a) and saturated (b) light response functions. For the simulation of the incident light, actual values of direct and diffuse PAR were taken from the INRAE weather station at Avignon on July 2023. The 3D Scenes were constructed with a density of 12 plants m^{-2} and inter-row spacing of 0.4 m. The lines on each graph describe the respective light-response curve. To improve the readability of the distribution, the right y-axis is logarithmic.

saturated light-response curve, the highest canopy-level photosynthesis can be achieved by avoiding leaf area in the interval of PPFD where co-limitation between carboxylation and electron transport occurs (i.e. the local slope between PPFD and instantaneous leaf-level photosynthesis decreases). This is illustrated in Fig. 14b: in the ideotype identified from the saturated response curve, the amount of leaf area at PPFD >500 μmol m^{-2} s^{-1} diminishes as the slope between PPFD and leaf-level photosynthesis decreases. Such an arrangement of leaf area seems reasonable, since over-exposed leaves will increase drastically mutual shading (leaves normal are more perpendicular to the sun direction), while their photosynthesis rates are only slightly higher as compared to less-exposed leaves. Average leaf inclination (ALA) is the main architectural variable that regulates this distribution of light intensity (Fig. 9). For that reason, under non-linear light-response curves, plants with more erectophile leaves, such as the architectural ideotype identified, will lead to higher canopy photosynthesis. According to our analysis, the lower the co-limitation point between carboxilation and electron transport is, the higher leaf inclination (e.g. low ALA) should be to maximize canopy photosynthesis.

In our analysis on the effect of plant architecture in canopy photosynthesis, we have assumed that the maize light-response curves –both non saturated and saturated– are constant, whereas they vary substantially in both, space and time. Light-response curves vary as a mechanism of adaptation to the local environment: temperature, water stress, leaf nitrogen and chlorophyll content or incoming light differences between upper and lower parts of the canopies. Considering such variability of the light-response function, finding an optimal plant architecture in actual field conditions is not straightforward. However, our results indicate that a non-linearity of the light-response curve has to be taken into account when analyzing the effect of plant architecture in canopy-level productivity. Only when considering the saturated light-response curve, the architectural ideotype identified resembles -mainly on ALA- to the five maize hybrids studied in the field, as shown in Fig. 15. A plant architecture with low ALA -i.e. more erect leaves- is only efficient when the response of leaf-level photosynthesis to light intensity is not linear. The resulting ideotype with more planophile leaves when considering a linear light-response, or when maximizing $fIPAR$ is unrealistic, and very different from modern maize architecture (Fig. 15). Furthermore, our results agree with the recent findings from Perez et al. (2019) on current commercial maize varieties. In their study (Perez et al., 2019) show that erectness has been indirectly selected over generations for its performance to improve yields, resulting in architectures favoring light distribution rather than light interception. In their analysis, modern cultivars show that light penetration enhances carbon availability to ears due to the absorbed light by the intermediate layers of the canopy (Cagnola et al., 2021).

Interestingly, among the architectural parameters that have more influence in canopy-level photosynthesis, leaves orientation play a minor role, as compared to leaf inclination. The ideotype defined from the light saturated scenario shows a marked leaves orientation around 45–50° relative the rows (Fig. 12) regardless of the sowing pattern. Such orientation would permit to balance the mutual shading between plants within the same rows and between adjacent rows. However, this contradicts what has been observed in studies (Maddonni et al., 2002, 2006; Serouart et al., 2023) who reported a systematic trend of maize to re-orient their leaves perpendicular to the row direction as the rectangularity of the sowing pattern increases. According to our analysis, the preferential orientation around 90° relative to rows does not improve light distribution nor canopy-level photosynthesis. A possible hypothesis that could explain it, is that leaves re-orientation constitutes, at least partially, a response of plants to local competition where they try to escape from their immediate neighbors, rather than a direct way of maximizing canopy-level light interception or distribution at whole plot level.

4.3. Opportunities to enhance canopy photosynthesis by adapting the sowing pattern

Beyond the plant architecture, the sowing pattern architecture is equally crucial and may have consequences on total canopy photosynthesis. Regardless of the light-response curve used for the simulations and the architectural ideotype, the results plotted in Fig. 13a–b clearly shows that higher canopy photosynthesis rates are achieved, for a given plant density, when the sowing pattern is squared. According to our analysis, decreasing row spacing would have always a positive impact in canopy photosynthesis as it reduces mutual shading between plants within the same row. This happens no matter what leaf orientation the plant is: random, or preferential at 45°. This would indicate that the benefit of decreasing row spacing to canopy-level photosynthesis would not depend on the ability of the cultivar to orient their leaves at a particular direction (Serouart et al., 2023). Highly rectangular patterns have therefore any advantage regarding light interception or light distribution. Moreover some research has demonstrated that narrowing row spacing to half the standard distance (i.e., to 0.4 m) reduced weed biomass by 39%–68% (Mhlanga et al., 2016) by reducing the amount of light reaching the bottom of the canopy in the middle of the inter-row

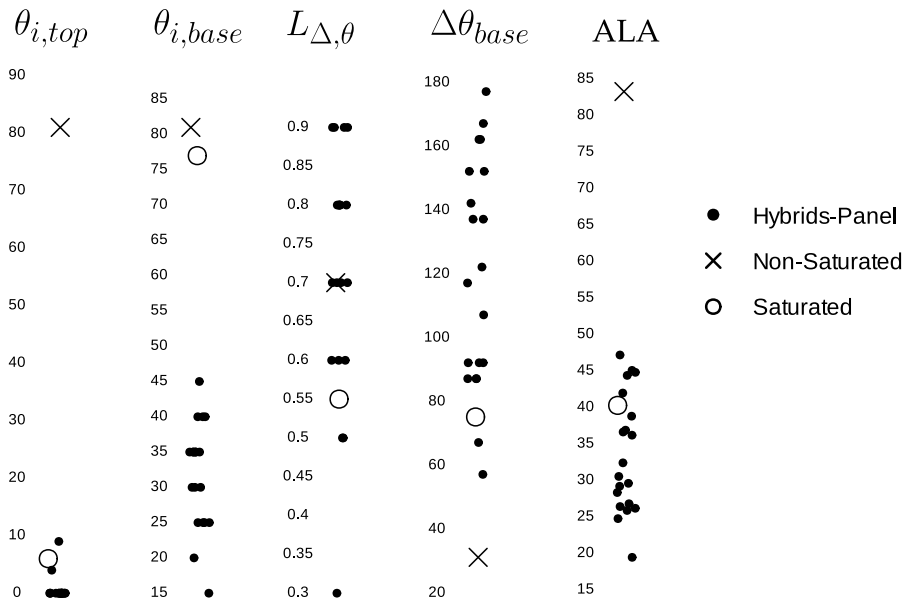

Fig. 15. CORNIBU architectural variables describing leaves inclination derived for the five actual maize hybrids studied in the Montardon experiment (considering the four sowing patterns per hybrid) and those from the most frequent maize ideotypes considering saturated and non-saturated light-response curves.

space (Tollenaar et al., 1994). This could also simultaneously benefit the plant in terms of water loss. Barbieri et al. (2012) demonstrated that reduced row spacing limited maize evapotranspiration and increased water use efficiency for grain production by up to 17%. Moreover, there may be a trade-off with soil water content, as narrow rows could lead to increased soil water depletion in the inter-row during the initial stages of crop growth, promoting water stress earlier in the season (Barbieri et al., 2012).

Regarding plant density, we find that its role on canopy photosynthesis depends on the linearity of the light-response curve. In the case of a non-saturated light response, the architectural ideotype has a planophile leaf inclination (Fig. 12b). For such an ideotype, increasing plant density produces a drastic augmentation of mutual shading that is not compensated by the photosynthesis in the most exposed leaves. Therefore, the optimal density would be around 6 plts m-^{2}, which is lower than the common practices in commercial fields (9–10 plts m-^{2}). By contrast, in the case of the erectophile ideotype given by the saturated light response, canopy-level photosynthesis is enhanced as plant density increases up to 9–10 plts m-^{2}. This reinforces our suggestion in Section 4.2 about the more realism of a saturated light-response curve as compared to the linear one. Moreover, these results are also in agreement with recent studies reporting yield differences around +1.0 to 2.0 t ha^{-1} for high density and low rectangularity (Maunas et al., 2018).

Our simulation study suggests a benefit in canopy-level photosynthesis of a squared sowing pattern. However, further works based on field experiments with a wide diversity of sowing patterns and maize hybrids are necessary to validate these findings. This study exclusively focuses on architecture, and variations in the stated propositions would emerge if genomics were considered in biomass production or yield. Recently, Song et al. (2023), estimates the contribution of canopy structure to photosynthesis between 5.3 to 6.7%. Notably, key factors such as Light Use Efficiency (LUE) or chlorophyll content, influencing both light absorbance and the photosynthetic efficiency of a leaf (Biswal et al., 2012), tend to have a larger effect on photosynthesis/biomass when different genotypes are compared.

5. Conclusion

In this study, we explored the relationship between maize architecture, sowing pattern, and canopy light regime using a new 3D model called CORNIBU. This model balances detailed architectural descriptions with a reduced number of input variables, allowing for easy exploration of phenotypic space. Digital canopies of five maize hybrids grown under different sowing patterns in a Montardon field trial (southwest France) were validated by comparing computed and actual daily $fIPAR$ values, showing a satisfactory fit ($R^2 \sim 0.6$).

An *in silico* experiment based on CORNIBU highlighted that leaf inclination variables contribute to 75%–85% of the variability in light interception ($fIPAR$) and distribution ($fILA$), with the remaining 15%–25% due to leaf orientation. Simulations revealed that the shape of the photosynthetic light-response curve influences the optimal plant architecture for maximizing canopy photosynthesis. Ideotypes that focus on light interception (e.g., planophile leaves) perform better with linear light-response curves, while those balancing interception and distribution (e.g., erectophile leaves) are optimal for non-linear curves, similar to current hybrids.

Additionally, we quantified the impact of sowing patterns on $fIPAR$, $fILA$ and photosynthesis, finding that reducing row spacing improves light distribution -by reducing mutual shading- and canopy photosynthesis. This supports previous findings that shifting from traditional rectangular patterns (between 0.7 and 0.8 m) to more squared/homogeneous spacing (between 0.4–0.5 m) could enhance maize yield (Testa et al., 2016; Gao et al., 2021).

CRediT authorship contribution statement

Mario Serouart: Writing – review & editing, Writing – original draft, Visualization, Resources, Methodology, Investigation, Data curation, Conceptualization. **Raúl López-Lozano:** Writing – review & editing, Writing – original draft, Supervision, Methodology, Investigation, Conceptualization. **Brigitte Escale:** Resources, Investigation. **Maëva Baumont:** Resources, Investigation. **Jean-Charles Deswarte:** Project administration. **Lucas Samatan Bernigaud:** Resources. **Marie Weiss:** Writing – review & editing, Software, Resources. **Benoit de Solan:** Visualization, Project administration, Methodology, Conceptualization.

Declaration of competing interest

The authors declare that they have no known competing financial interests or personal relationships that could have appeared to influence the work reported in this paper.

Acknowledgments

We would like to express our gratitude to Shouyang Liu for providing the D3P raw environment, which greatly helped for the bash-processing with POVray to generate synthetic hemispherical images. We would also like to acknowledge Micheline Debroux, Côme Amilhastre and Juliette Boron for their valuable annotations and skeleton frameworks, which significantly contributed to the clarity of our research. Additionally, we extend our appreciation to Christian Fournier, Raphaël P.A. Perez, and Romain Barillot for their indirect contributions in providing resources (especially pyCaribu and hmba repositories). Finally, we acknowledge Albert Olioso (UR URFM, INRAE, Avignon) for his insightful comments on the manuscript.

This work received support from ANRT for the CIFRE grant of Mario Serouart, cofunded by INRAE and Arvalis. The study was partly supported by several projects including ANR PHENOME (Programme d'investissement d'avenir), Digitag (PIA Institut Convergences Agriculture Numérique ANR-16-CONV-0004) and CASDAR LITERAL. The authors thank the INRAE EMMAH laboratory at Avignon (France) in charge of the "Flux and Remote Sensing site" for the supply of the data.

Appendix A. Supplementary data

Supplementary material related to this article can be found online at https://doi.org/10.1016/j.compag.2024.109694.

Data availability

The 3D maize model developed in this study, linked with Caribu, is named CORNIBU and is available at: https://github.com/mserouar/CORNIBU (+ all other data once published)

References

Barbieri, Pablo, Echarte, Laura, Maggiora, A., Sadras, Victor, Echeverría, Hernan, Andrade, Fernando, 2012. Maize evapotranspiration and water-use efficiency in response to row spacing. Agron. J. 104, 939. http://dx.doi.org/10.2134/agronj2012.0014.

Baret, Frederic, Madec, Simon, Irfan, Kamran, Lopez, Jeremy, Comar, Alexis, Hemmerlé, Matthieu, Dutartre, Dan, Praud, Sebastien, Tixier, Marie Helene, 2018. Leaf-rolling in maize crops: From leaf scoring to canopy-level measurements for phenotyping. J. Exp. Bot. (ISSN: 1460-2431) 69 (10), 2705–2716. http://dx.doi.org/10.1093/jxb/ery071.

Berzsenyi, Z., Tokatlidis, I.S., 2012. Density dependence rather than maturity determines hybrid selection in dryland maize production. Agron. J. (ISSN: 1435-0645) 104 (2), 331–336. http://dx.doi.org/10.2134/agronj2011.0205.

Biswal, Ajaya K., Pattanayak, Gopal K., Pandey, Shiv S., Leelavathi, Sadhu, Reddy, Vanga S., Govindjee, Tripathy, Baishnab C., 2012. Light intensity-dependent modulation of chlorophyll *b* biosynthesis and photosynthesis by overexpression of chlorophyllide *a* oxygenase in tobacco. Plant Physiol. (ISSN: 1532-2548) 159 (1), 433–449. http://dx.doi.org/10.1104/pp.112.195859.

Boudon, Frederic, Fournier, Christian, Perez, Raphael, Pradal, Christophe, Pallas, Benoit, 2020. Openalea-training/hmba312_training. URL https://github.com/openalea-training/hmba312_training.

Cagnola, Juan, Parco, Martin, Rotili, Diego, Ploschuk, Edmundo, Curin, Facundo, Amas, Juan, Luque, Sergio, Maddonni, Gustavo, Otegui, María, Casal, Jorge, 2021. Artificial selection for grain yield has increased net CO2 exchange of the ear leaf in maize crops. J. Exp. Bot. 72, http://dx.doi.org/10.1093/jxb/erab119.

Carnell, Rob, 2022. Lhs: Latin hypercube samples.

Chelle, Michael, Andrieu, Bruno, 1998. The nested radiosity model for the distribution of light within plant canopies. Ecol. Model. (ISSN: 03043800) 111 (1), 75–91. http://dx.doi.org/10.1016/S0304-3800(98)00100-8.

Collison, Robert F., Raven, Emma C., Pignon, Charles P., Long, Stephen P., 2020. Light, not age, underlies the maladaptation of maize and miscanthus photosynthesis to self-shading. Front. Plant Sci. (ISSN: 1664-462X) 11, http://dx.doi.org/10.3389/fpls.2020.00783.

Dulk, Jan Arie den, 1989. The Interpretation of Remote Sensing: A Feasibility Study. Wageningen, ISBN: 978-90-90-02707-4.

Eliazer Nelson, Ann Raeboline Lincy, Ravichandran, Kavitha, Antony, Usha, 2019. The impact of the green revolution on indigenous crops of India. J. Ethnic Foods (ISSN: 2352-6181) 6 (1), 8. http://dx.doi.org/10.1186/s42779-019-0011-9.

España, Marisa, Frederic, Baret, Chelle, Michael, Aries, Frank, Andrieu, Bruno, 1998. A dynamic model of maize 3D architecture: Application to the parameterisation of the clumpiness of the canopy. Agronomie 18, 609–626. http://dx.doi.org/10.1051/agro:19981001.

Faivre, Robert, Iooss, Bertrand, Mahévas, Stéphanie, Makowski, David, Monod, Herve, 2013. Analyse de Sensibilité et Exploration de Modèles. In: Collection Savoir-Faire, Editions Quae.

FAO, 2023. FAO Cereal Supply and Demand Brief. Food and Agriculture Organization of the United Nations.

Farquhar, G.D., von Caemmerer, S., Berry, J.A., 1980. A biochemical model of photosynthetic CO2 assimilation in leaves of c 3 species. Planta (ISSN: 0032-0935) 149 (1), 78–90. http://dx.doi.org/10.1007/BF00386231.

Fournier, Christian, Andrieu, Bruno, 1998. A 3D architectural and process-based model of maize development. Ann. Botany 81, 233–250. http://dx.doi.org/10.1006/anbo.1997.0549.

Fournier, Christian, Boudon, Frédéric, Chelle, Michaël, Saudreau, M, Ngao, Jérôme, Louarn, Gaëtan, Combes, Didier, Pradal, Christophe, 2016. Toward the inter-comparison of radiation transfert model for plant modelling application. In: Poster 2016 IEEE International Conference on Functional-Structural Plant Growth Modeling, Simulation, Visualization and Applications. FSPMA 2016.

Gao, Jia, Lei, Ming, Yang, Luojin, Wang, Pu, Tao, Hongbin, Huang, Shoubing, 2021. Reduced row spacing improved yield by optimizing root distribution in maize. Eur. J. Agron. (ISSN: 1161-0301) 127, 126291. http://dx.doi.org/10.1016/j.eja.2021.126291.

Jin, Shichao, Su, Yanjun, Gao, Shang, Wu, Fangfang, Hu, Tianyu, Liu, Jin, Li, Wenkai, Wang, Dingchang, Chen, Shaojiang, Jiang, Yuanxi, Pang, Shuxin, Guo, Qinghua, 2018a. Deep learning: Individual maize segmentation from terrestrial lidar data using faster R-CNN and regional growth algorithms. Front. Plant Sci. 9, http://dx.doi.org/10.3389/fpls.2018.00866.

Jin, Shichao, Su, Yanjun, Wu, Fangfang, Pang, Shuxin, Gao, Shang, Hu, Tianyu, Liu, Jin, Guo, Qinghua, 2018b. Stem-leaf segmentation and phenotypic trait extraction of individual maize using terrestrial LiDAR data. IEEE Trans. Geosci. Remote Sens. PP, 1–11. http://dx.doi.org/10.1109/TGRS.2018.2866056.

Khan, Faheem, Mukhtar, Irem, Batool, Noreen, 2013. A unified interpolating subdivision scheme for curves/surfaces by using Newton interpolating polynomial. OJAppS 03 (03), 263–269. http://dx.doi.org/10.4236/ojapps.2013.33033, (ISSN: 2165-3917, 2165-3925).

Li, Rongfa, Zhang, Guoqiang, Xie, Ruizhi, Hou, Peng, Ming, Bo, Xue, Jun, Wang, Keru, Li, Shaokun, 2021. Optimizing row spacing increased radiation use efficiency and yield of maize. Agron. J. (ISSN: 1435-0645) 113 (6), 4806–4818. http://dx.doi.org/10.1002/agj2.20828.

López-Lozano, Raúl, Baret, Frédéric, Chelle, Michaël, Rochdi, Nadia, España, Marisa, 2007. Sensitivity of gap fraction to maize architectural characteristics based on 4D model simulations. Agricult. Forest. Meterol. (ISSN: 01681923) 143 (3–4), 217–229. http://dx.doi.org/10.1016/j.agrformet.2006.12.005.

Maddonni, G.A, Chelle, M., Drouet, J.-L, Andrieu, B., 2001a. Light interception of contrasting azimuth canopies under square and rectangular plant spatial distributions: Simulations and crop measurements. Field Crops Res. (ISSN: 03784290) 70 (1), 1–13. http://dx.doi.org/10.1016/S0378-4290(00)00144-1.

Maddonni, Gustavo A., Cirilo, Alfredo G., Otegui, M.E., 2006. Row width and maize grain yield. Agron. J. 98 (6), 1532–1543. http://dx.doi.org/10.2134/agronj2006.0038, (ISSN: 0002-1962, 1435-0645).

Maddonni, Gustavo Angel, Otegui, María Elena, Andrieu, Bruno, Chelle, Michael, Casal, Jorge J., 2002. Maize leaves turn away from neighbors. Plant Physiol. 130 (3), 1181–1189. http://dx.doi.org/10.1104/pp.009738, (ISSN: 1532-2548, 0032-0889).

Maddonni, G.A, Otegui, M.E, Cirilo, A.G, 2001b. Plant population density, row spacing and hybrid effects on maize canopy architecture and light attenuation. Field Crops Res. (ISSN: 03784290) 71 (3), 183–193. http://dx.doi.org/10.1016/S0378-4290(01)00158-7.

Madec, Simon, Irfan, Kamran, Velumani, Kaaviya, Baret, Frederic, David, Etienne, Daubige, Gaetan, Samatan, Lucas Bernigaud, Serouart, Mario, Smith, Daniel, James, Chrisbin, Camacho, Fernando, Guo, Wei, De Solan, Benoit, Chapman, Scott C., Weiss, Marie, 2023. VegAnn, vegetation annotation of multi-crop RGB images acquired under diverse conditions for segmentation. Sci. Data (ISSN: 2052-4463) 10 (1), 302. http://dx.doi.org/10.1038/s41597-023-02098-y, Number: 1 Publisher: Nature Publishing Group.

Maunas, L., Escale, B., Espagnol, G., 2018. Maize sowing: Density and spacing determine yield. In: Perspectives Agricoles n° 454.

Mhlanga, Blessing, Chauhan, Bhagirath Singh, Thierfelder, Christian, 2016. Weed management in maize using crop competition: A review. Crop Prot. (ISSN: 0261-2194) 88, 28–36. http://dx.doi.org/10.1016/j.cropro.2016.05.008.

Perez, Raphaël P.A., Fournier, Christian, Cabrera-Bosquet, Llorenç, Artzet, Simon, Pradal, Christophe, Brichet, Nicolas, Chen, Tsu-Wei, Chapuis, Romain, Welcker, Claude, Tardieu, François, 2019. Changes in the vertical distribution of leaf area enhanced light interception efficiency in maize over generations of selection. Plant Cell Environ. (ISSN: 1365-3040) 42 (7), 2105–2119. http://dx.doi.org/10.1111/pce.13539.

Perez, Raphaël P.A., Pallas, Benoît, Le Moguédec, Gilles, Rey, Hervé, Griffon, Sébastien, Caliman, Jean-Pierre, Costes, Evelyne, Dauzat, Jean, 2016. Integrating mixed-effect models into an architectural plant model to simulate inter- and intra-progeny variability: A case study on oil palm (elaeis guineensis jacq). J. Exp. Bot. (ISSN: 0022-0957) 67 (15), 4507–4521. http://dx.doi.org/10.1093/jxb/erw203.

Persistence of Vision Pty. Ltd., 2013. Persistence of vision raytracer (version 3.7).

Ritchie, S.W., Hanway, J.J., 1982. How a corn plant develops.

Sangoi, Luis, 2001. Understanding plant density effects on maize growth and development: An important issue maximizes grain yield. Ciencia Rural - CIENC RURAL 31, http://dx.doi.org/10.1590/S0103-84782001000100027.

SciPy, 2020. Scipy 1.0: Fundamental algorithms for scientific computing in python. Nat. Methods 17, 261–272. http://dx.doi.org/10.1038/s41592-019-0686-2.

Serouart, Mario, López-Lozano, Raúl, Daubige, Gaëtan, Baumont, Maëva, Escale, Brigitte, De Solan, Benoit, Baret, Frédéric, 2023. Analyzing changes in maize leaves orientation due to GxExM using an automatic method from RGB images. Plant Phenom. (ISSN: 2643-6515) 5, 0046. http://dx.doi.org/10.34133/plantphenomics.0046.

Serouart, Mario, Madec, Simon, David, Etienne, Velumani, Kaaviya, López-Lozano, Raúl, Weiss, Marie, Baret, Frédéric, 2022. SegVeg: Segmenting RGB images into green and senescent vegetation by combining deep and shallow methods. Plant Phenom. (ISSN: 2643-6515) 2022, http://dx.doi.org/10.34133/2022/9803570, 2022/9803570.

Sharratt, Brenton S., McWilliams, Denise A., 2005. Microclimatic and rooting characteristics of narrow-row versus conventional-row corn. Agron. J. 97 (4), 1129–1135. http://dx.doi.org/10.2134/agronj2004.0292, (ISSN: 0002-1962, 1435-0645).

Song, Qingfeng, Liu, Fusang, Bu, Hongyi, Zhu, Xin-Guang, 2023. Quantifying contributions of different factors to canopy photosynthesis in two maize varieties: Development of a novel 3D canopy modeling pipeline. Plant Phenom. (ja), http://dx.doi.org/10.34133/plantphenomics.0075, Publisher: American Association for the Advancement of Science.

Su, Yanjun, Wu, Fangfang, Ao, Zurui, Jin, Shichao, Qin, Feng, Liu, Boxin, Pang, Shuxin, Liu, Lingli, Guo, Qinghua, 2019. Evaluating maize phenotype dynamics under drought stress using terrestrial lidar. Plant Methods 15, http://dx.doi.org/10.1186/s13007-019-0396-x.

Tang, Boxin, 1993. Orthogonal array-based latin hypercubes. J. Amer. Statist. Assoc. (ISSN: 0162-1459) 88 (424), 1392–1397. http://dx.doi.org/10.2307/2291282, Publisher: [American Statistical Association, Taylor & Francis, Ltd.].

Testa, Giulio, Reyneri, Amedeo, Blandino, Massimo, 2016. Maize grain yield enhancement through high plant density cultivation with different inter-row and intra-row spacings. Eur. J. Agron. (ISSN: 11610301) 72, 28–37. http://dx.doi.org/10.1016/j.eja.2015.09.006.

Timlin, Dennis J., Fleisher, David H., Kemanian, Armen R., Reddy, Vangimalla R., 2014. Plant density and leaf area index effects on the distribution of light transmittance to the soil surface in maize. Agron. J. 106 (5), 1828–1837. http://dx.doi.org/10.2134/agronj14.0160, (ISSN: 0002-1962, 1435-0645).

Tollenaar, M., Dibo, A.A., Aguilera, A., Weise, S.F., Swanton, C.J., 1994. Effect of crop density on weed interference in maize. Agron. J. (ISSN: 1435-0645) 86 (4), 591–595. http://dx.doi.org/10.2134/agronj1994.00021962008600040003x.

Wang, Juhui, Faivre, Robert, Richard, Hervé, Monod, Hervé, 2015. mtk: A general-purpose and extensible R environment for uncertainty and sensitivity analyses of numerical experiments. R J. (ISSN: 2073-4859) 7 (2), 206. http://dx.doi.org/10.32614/RJ-2015-031.

Wang, Zhenchang, Kang, Shaozhong, Jensen, Christian, Liu, Fulai, 2012. Alternate partial root-zone irrigation reduces bundle-sheath cell leakage to CO2 and enhances photosynthetic capacity in maize leaves. J. Exp. Bot. 63, 1145–1153. http://dx.doi.org/10.1093/jxb/err331.

Willey, R.W., Heath, S.B., 1969. The quantitative relationships between plant population and crop yield. In: Brady, N.C. (Ed.), Advances in Agronomy. vol. 21, Academic Press, pp. 281–321. http://dx.doi.org/10.1016/S0065-2113(08)60100-5.

Xiao, Shunfu, Ye, Yulu, Fei, Shuaipeng, Haochong, Chen, Zhang, Bingyu, Qing, Li, Cai, Zhibo, Che, Yingpu, Wang, Qing, Ghafoor, Abu Zar, Bi, Kaiyi, Shao, Ke, Wang, Ruili, Guo, Yan, Baoguo, Li, Zhang, Rui, Chen, Zhen, Ma, Yuntao, 2023. High-throughput calculation of organ-scale traits with reconstructed accurate 3D canopy structures using a UAV RGB camera with an advanced cross-circling oblique route. ISPRS J. Photogramm. Remote Sens. 201, 104–122. http://dx.doi.org/10.1016/j.isprsjprs.2023.05.016.

Yin, X., Struik, P.C., 2009. C3 and C4 photosynthesis models: An overview from the perspective of crop modelling. NJAS - Wageningen J. Life Sci. (ISSN: 1573-5214) 57 (1), 27–38. http://dx.doi.org/10.1016/j.njas.2009.07.001, Recent Advances in Crop Growth Modelling.